

Task 1.1

Title

Resource exploration and characterization

Projects (presented on the following pages)

Wireline logging of Bedretto stress measurement boreholes – preliminary results

Eva Caspari, Andrew Greenwood, Ludovic Baron, Klaus Holliger

Numerical simulation of seismic wave dispersion and attenuation due to squirt flow

Yury Alkhimenkov, Eva Caspari, Nicolás D. Barbosa, Beatriz Quintal

Regional-scale flow models of the orogenic hydrothermal system at Grimsel Pass, Switzerland

Peter Alt-Epping, Larry W. Diamond, Christoph Wanner

Reliability of calibration and prediction of borehole failure models

Asmae Dahrabou, Benoît Valley, Philip Brunner, Andres Alcolea, Peter Meier

Application of Chemostratigraphy and petrology to characterize the Reservoirs of The Mesozoic sequence crossed by the Geo-01 well: potential for direct heat production and heat-storage

G. Ferreira De Oliveira, A. De Haller, L. Guglielmetti, Y. Makhlou, A. Moscariello

Hydraulic Characterization of the Bedretto Underground Laboratory

Nima Gholizadeh Doonechaly, Nathan Dutler, Bernard Brixel, Marian Hertrich, Simon Loew

Monitoring and Flow Path Reconstruction of Saline Tracer Tests with GPR

Peter-Lasse Giertzuch, Joseph Doetsch, Mohammadreza Jalali, Alexis Shakas, Cédric Schmelzbach, Hansruedi Maurer

Borehole radar and full waveform sonic measurements of the Bedretto stressmeasurement boreholes

Andrew Greenwood, Eva Caspari, Ludovic Baron, Klaus Holliger

Geochemical Characterization of Geothermal Waters Circulation in Carbonatic Geothermal Reservoirs of the Geneva Basin (GB)

L. Guglielmetti, F. Eichinger, A. Moscariello

Bayesian inversion of tube waves to estimate fracture aperture and compliance: Application to a real dataset

Jürg Hunziker, Andrew Greenwood, Shohei Minato, Nicolas Barbosa, Eva Caspari, Klaus Holliger

In-situ stress estimation from fault slip triggered during fluid injection

Maria Kakurina, Yves Guglielmi, Christophe Nussbaum, Benoît Valley

Rock mechanics properties for fractured limestone hydrothermal system

Morgane Koumrouyan, Reza Sohrabi, Benoît Valley

Determine fault criticality using seismic monitoring and fluid pressure analysis

Léa Perrochet, Giona Preisig, Benoît Valley

Anomalous Vp/Vs in pressurized reservoirs: Does it exist and what does it entail?

Lucas Pimienta, Beatriz Quintal, Eva Caspari, Marie Violay

Effects of fracture connectivity on Rayleigh wave dispersion

Gabriel Quiroga, J. Germán Rubino, Santiago Solazzi, Nicolás Barbosa, Klaus Holliger

Seismic signatures of porous rocks containing partially saturated fracture networks

Santiago G. Solazzi, Jürg Hunziker, Eva Caspari, Marco Favino, Klaus Holliger

Poroelastic effects of the damaged zone on fracture reflectivity

Edith Sotelo, Santiago G. Solazzi, J. Germán Rubino, Nicolás D. Barbosa, Klaus Holliger

Where are the favorable locations for deep geothermal in Switzerland?

Benoît Valley, Stephen A. Miller

Geochemical evidence for large-scale and long-term topographydriven groundwater flow in orogenic crystalline basements

Christoph Wanner, H. Niklaus Waber, Kurt Bucher



Wireline logging of Bedretto stress measurement boreholes - preliminary results

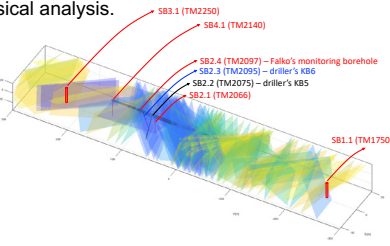
Eva Caspari, Andrew Greenwood, Ludovic Baron and Klaus Holliger

Summary

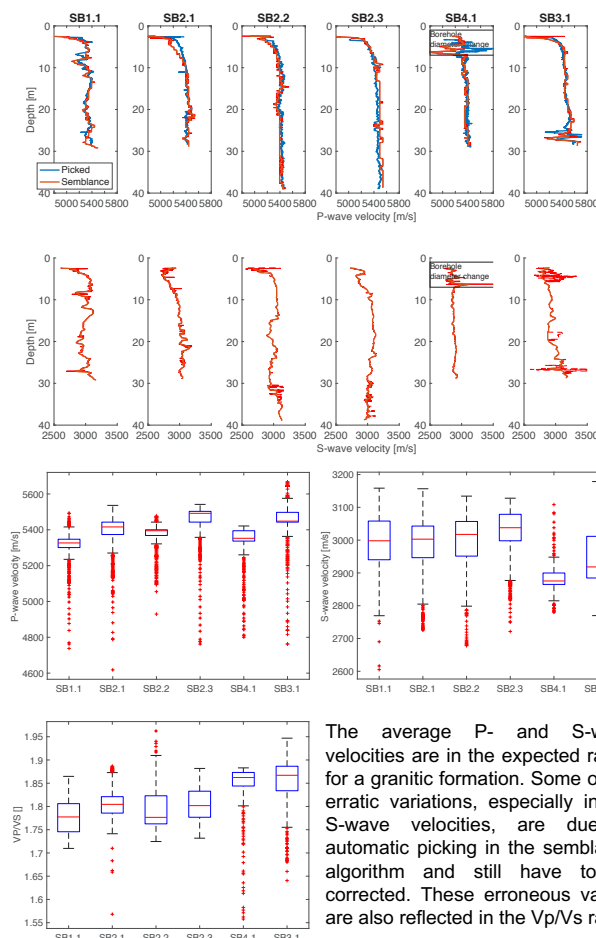
A set of geophysical wireline logs, comprising optical and acoustic televiewer data (OTV and ATV), full waveform sonic (FWS), normal resistivity (N08, N16, N32, N64), fluid temperature and conductivity (FTC), natural gamma (NG), spectral gamma (SGR), and borehole radar (BHR) were collected in 6 stress measurements boreholes in the Bedretto underground laboratory. The laboratory is situated in the crystalline basement of the Gotthard massif and the prevailing rock type is the Rotondo granite. The purpose of the logging campaign was twofold:

- 1) characterization of the rock mass in preparation for mini-frac and hydraulic shearing stress measurements and associated induced fractures
 - 2) in-depth analysis of the petrophysical properties of the rock mass
- Here, we show a selection of the log data which will be utilized for the petrophysical analysis.

The sketch shows the location of the stress measurement boreholes and slip surfaces mapped along the tunnel. (Courtesy Xiaodong Ma)

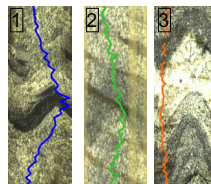
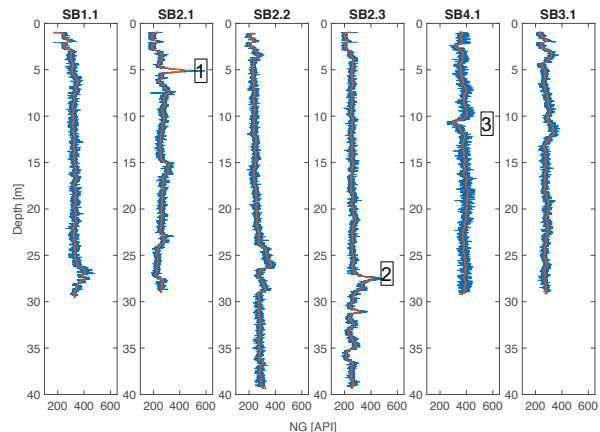


FWS - velocities



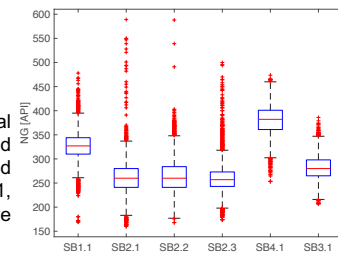
The average P- and S-wave velocities are in the expected range for a granitic formation. Some of the erratic variations, especially in the S-wave velocities, are due to automatic picking in the semblance algorithm and still have to be corrected. These erroneous values are also reflected in the Vp/Vs ratio.

Natural gamma

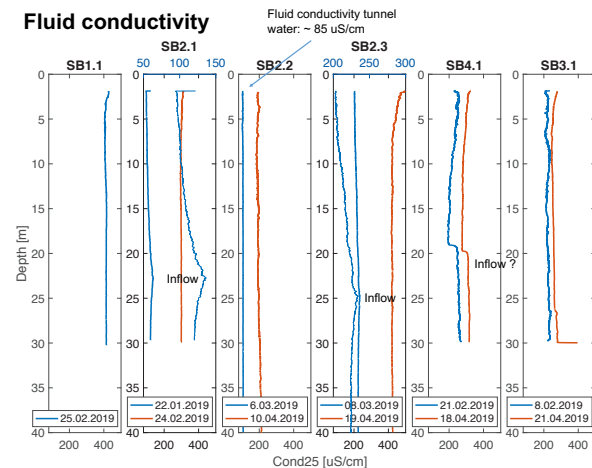


Strong variations in the natural gamma logs are likely to be associated with variations in Biotite content (1 and 2) and Quartz veins (3).

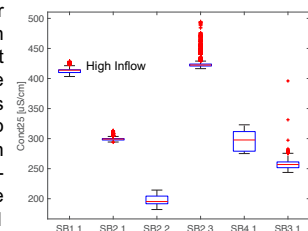
The highest average natural gamma readings as indicated by the boxplots are observed in borehole SB1.1 and SB 4.1, which are otherwise relative homogeneous.



Fluid conductivity



All boreholes were flushed after drilling with tunnel water, which originates from in-flow through fault zones. The fluid conductivity of the tunnel water is ~ 85 uS/m, which is considerably different with regard to the fluid conductivity measured in all boreholes after some equilibration time. At the time these measurements were taken, SB1.1 and SB2.3 were probably closest to their natural ambient state.



Acknowledgement: We thank Benoît Valley from the University of Neuchâtel for providing logging equipment and support and the BULG team for their support.

Numerical simulation of seismic wave dispersion and attenuation due to squirt flow

Yury Alkhimenkov^{12*}, Eva Caspari¹, Nicolás D. Barbosa³, Beatriz Quintal¹
¹*Institute of Earth Sciences, University of Lausanne, Switzerland,* ²*Swiss Geocomputing Centre, University of Lausanne, Switzerland,* ³*University of Geneva, Switzerland*

Introduction

One of the major causes of seismic wave attenuation and velocity dispersion in fluid-saturated porous media is the local flow induced by a passing wave. Local flow at the microscopic scale is referred to as squirt flow and occurs in very compliant pores such as grain contacts or microcracks which are connected to other less compliant pores [1, 2].

In this study, we perform a 3D numerical simulation of squirt flow using a finite element approach. We obtain frequency-dependent effective properties of a porous medium and calculate dispersion and attenuation due to fluid flow from a compliant crack to a stiff pore. We compare our numerical simulation with an existing analytical squirt flow model [3].

Theory

We consider a two phase medium composed by a solid phase (grains) and a fluid-saturated pore space. Grains are described as a linear isotropic elastic material for which the conservation of momentum is

$$\nabla \cdot \sigma = 0, \quad (1)$$

where σ is the stress tensor. The stress-strain relation is written as

$$\sigma = \mathbf{C} : \epsilon, \quad (2)$$

where ϵ is the strain tensor and \mathbf{C} is the isotropic stiffness tensor, whose components are fully described by bulk K and shear μ moduli.

A fluid phase is described by the quasi-static linearised compressible Navier-Stokes momentum equation [4]:

$$-\nabla p + \eta \nabla^2 v + \frac{1}{3} \eta \nabla (\nabla \cdot v) = 0, \quad (3)$$

where v is the particle velocity and η is the shear viscosity. Equation (3) is valid for the laminar flow of a Newtonian fluid. In our simulation the energy dissipation is caused only by fluid pressure diffusion because inertial effects are neglected [5].

Acknowledgements

This research is funded by the Swiss National Science Foundation. Yury Alkhimenkov thanks Dr. J. Hunziker for technical support, Dr. B. Gurevich and Dr. S. Glubokovskikh for stimulating discussions and Dr. M. Klepikova for the template.

Numerical methodology

In this study, we consider a 3D numerical model of a flat cylinder whose edges are connected with a torus. Topologically these two geometries represent one domain.

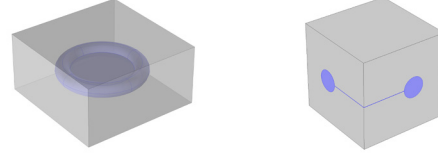


Figure 1: (Left) Sketch illustrating a flat cylinder representing a crack whose edges are connected with a torus (a stiff pore). The blue region represents the pore space saturated with a fluid, the transparent gray area corresponds to the solid grain material; (Right) Sketch showing a quarter of the model.

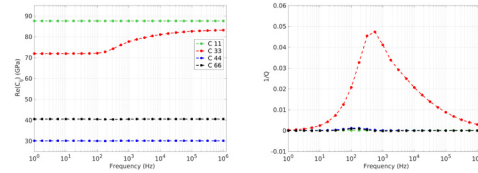


Figure 2: Numerical results for the C_{ij} components: (left) Real part of the C_{ij} components and (right) dimensionless attenuation for the corresponding C_{ij} components.

Comparison to an analytical model

$Z_n Q - Z_t Q$ model: the difference between "a torus embedded into the solid grain material (VTI_1)" compliance tensor and "a crack embedded into a medium described by the VTI_1" compliance tensor.

$Z_n D - Z_t D$ model: the difference between the VTI_1 compliance tensor and "a torus connected with a crack embedded into the grain material" compliance tensor.

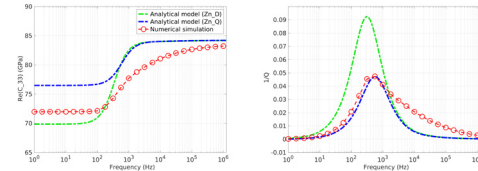


Figure 3: Real part of the C_{33} component and dimensionless attenuation for the C_{33} component.

Conclusion

We calculated the frequency-dependent effective properties of a fluid-saturated porous medium due to squirt fluid flow. While our numerical results are consistent with the current physical understanding of the squirt flow impact on the velocity dispersion and wave attenuation, some new features have been found. We confirmed that the attenuation is controlled by the length of a fluid path but dispersion is controlled by the combined compliances of the crack connected to the stiffer pore which hasn't been taken into account in analytical models. However, the observed discrepancy between the analytical and numerical solutions tends to become smaller as the aspect ratio of the crack and the minor radius of the torus (representing spherical pores) is decreased.


References

- [1] William F Murphy, Kenneth W Winkler, and Robert L Kleinberg. Acoustic relaxation in sedimentary rocks: Dependence on grain contacts and fluid saturation. *Geophysics*, 51(3):757–766, 1986.
- [2] Boris Gurevich, Dina Makarynska, Osni Bastos de Paula, and Marina Pervukhina. A simple model for squirt-flow dispersion and attenuation in fluid-saturated granular rocks. *Geophysics*, 75(6):N109–N120, 2010.
- [3] Olivia Collet and Boris Gurevich. Frequency dependence of anisotropy in fluid saturated rocks—part i: aligned cracks case. *Geophysical Prospecting*, 64(4):1067–1084, 2016.
- [4] LD Landau and EM Lifshitz. *Course of theoretical physics. vol. 6: Fluid mechanics*. London, 1959.
- [5] Beatriz Quintal, J Germán Rubino, Eva Caspari, and Klaus Holliger. A simple hydromechanical approach for simulating squirt-type flow. *Geophysics*, 81(4):D335–D344, 2016.

Regional-scale flow models of the orogenic hydrothermal system at Grimsel Pass, Switzerland

Peter Alt-Epping, Larryn W. Diamond & Christoph Wanner
 Rock-Water Interaction, Institute of Geological Sciences, University of Bern

Supported by:

 Schweizerische Eidgenossenschaft
 Confédération suisse
 Confederazione Svizzera
 Confederaziun svizra
 Swiss Confederation
 Innosuisse – Swiss Innovation Agency

u^b

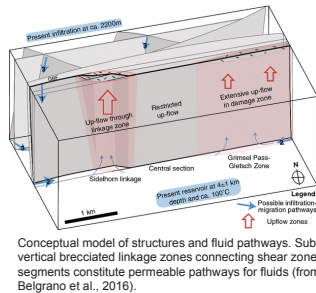
UNIVERSITÄT
BERN

1) Introduction

Thermal waters at temperatures ranging between 17 - 28 °C discharge at a rate of ≤ 10 L/min into a tunnel underneath Grimsel Pass (2164 m) in the Central Alps. Fluid discharge occurs at the intersection with a brecciated fault zone (Grimsel Breccia Fault (GBF)), a late Neogene exhumed strike-slip fault (Belgrano et al., 2016). The chemical composition of the water sampled in the tunnel shows that the water is a mixture of old geothermal water and younger cold water. Both components have meteoric isotope signatures, but the thermal water is derived from a higher altitude. Residence times of the old and young waters are ≤ 30 ky and ~ 7 years, respectively (Waber et al., 2017).

Results from Na-K geothermometry on present-day fluid samples indicate the maximum temperature at depth could be as high as 250 °C. Given the local geothermal gradient this corresponds to a circulation depth of meteoric water to at least 9 km (Diamond et al., 2018). These results imply that little or no fluid-rock interaction or fluid mixing occurred during the ascent of the hot fluid.

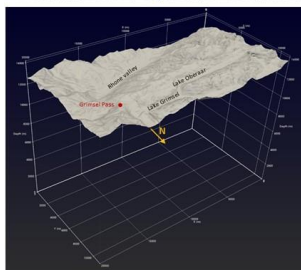
The breccia in the GBF has a sub-vertical, pipe-like structure in 3D, and constitutes a permeable linkage zone between parallel segments of the main shear-zone. Another such linkage zone exists in the Sidelhorn area to the west (Belgrano et al., 2016). Thus, it can be expected that these permeable linkage zones are common structural features along the fault.



2) Numerical model

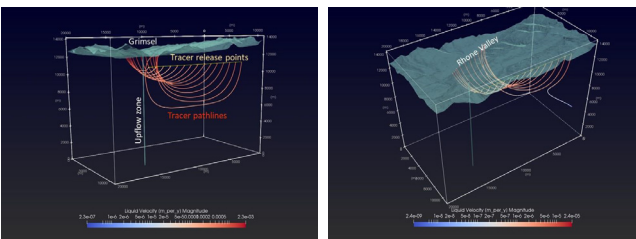


We use numerical modelling to better understand the regional flow system in the Grimsel area that leads to discharge of thermal water at Grimsel Pass. The model incorporates the topography of the region as its top boundary and extends to a depth of 12.5 km. The upflow zone at Grimsel Pass is incorporated as a vertical permeable conduit ($k = 1e-13$ m²) within a low permeability granitic rock ($k = 3e-20$ m²). The model is composed of 3.9 Mio. cells. Simulations were carried out with the high performance reactive transport code PFLOTRAN (www.pflotran.org) on UBELIX, the HPC cluster at the University of Bern



3) Results

- What is the role of the GBF in generating upflow under Grimsel Pass?

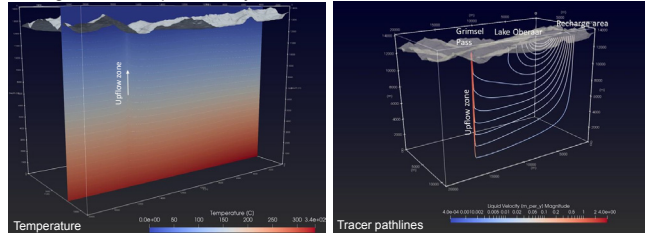


The GBF, if represented as an unconfined, permeable vertical plane extending into the high mountains towards the west and to a depth of 12.5 km, sustains hydrothermal upflow at Grimsel Pass. Without the GBF, deep groundwater discharges into the Rhone Valley.

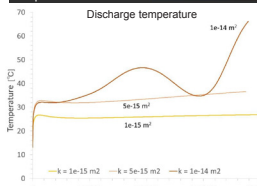
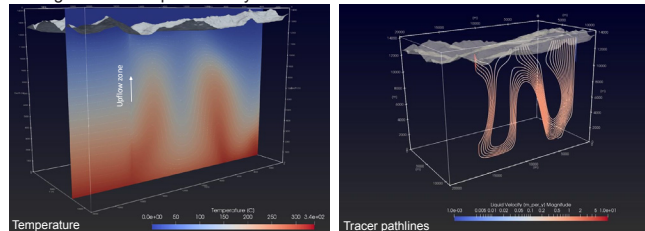
Results cont'd

- Can topography drive meteoric water to a depth > 9 km?

Homogeneous fault permeability $1e-15$ m²



Homogeneous fault permeability $1e-14$ m²

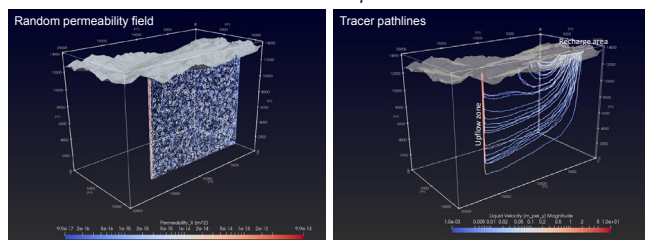


Simulations show that deep infiltration of meteoric water into the fault plane to a depth > 9 km, solely driven by topography and without permeability forcing, is possible. Models calibrated to match discharge rates and temperatures at the thermal springs suggest permeabilities of the GBF between $1e-15$ m² and $1e-14$ m² (fault width 100 m).

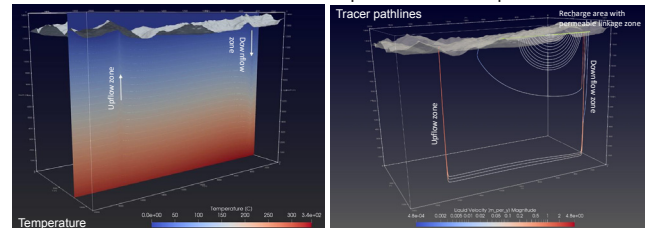
At permeabilities > $5e-15$ m², the flow system in the fault becomes unstable and convection cells form which induce transient flow and transient temperature conditions at the discharge site.

Under stable flow conditions significant fluid mixing along the upflow conduit occurs, which is inconsistent with geochemical evidence. Some permeability forcing is needed to focus flow into the deeper section of the upflow zone.

- What controls focused flow in the deep fault zone



Heterogeneity due to random permeability perturbations leads to flow channelling. It is possible that an (unknown) permeability distribution in the fault causes focused inflow into the deep section of the upflow zone.



Alternatively, permeable linkage zones causing upflow may also occur at higher altitude, inducing focused downflow and focused flow at depth.

REFERENCES

- Belgrano, T.M., Herwegh, M. & Berger, A., 2016. Inherited structural controls on fault geometry, architecture and hydrothermal activity, an example from Grimsel Pass, Switzerland, Swiss J. Geosci., 109, 345-364.
 Diamond, L.W., Wanner, C. & Alt-Epping, P., 2018. Penetration depth of meteoric water in orogenic geothermal systems. Geology, 46, 1063-1066.
 Waber, H.N., Schneeberger, R., Mäder, U.K., Wanner, C., 2017. Constraints on evolution and residence time of geothermal water in granitic rock at Grimsel (Switzerland), 15th Water-Rock Interaction Symposium, WRI-15, Procedia Earth and Planetary Science 17, 774-777

Reliability of calibration and prediction of borehole failure models

Asmae Dahrabou⁽¹⁾, Benoît Valley⁽¹⁾, Philip Brunner⁽¹⁾, Andres Alcolea⁽²⁾, Peter Meier⁽²⁾

⁽¹⁾ Centre for Hydrogeology and Geothermics, University of Neuchâtel, Emile-Argand 11, 2000-Neuchâtel, Switzerland.

⁽²⁾ Geo-Energie Suisse AG, Reitergasse 11, 8004 Zürich, Switzerland.

I- Project context and objectives

In the frame of a CTI-project, the CHYN and Geo-Energie Suisse AG are developing a workflow and associated software tools that allow a fast decision-making process for selecting an optimal well trajectory while drilling deep inclined wells for EGS-projects. The goal is to minimize borehole instabilities as it enhances drilling performance and maximize the intersection with natural fractures because it increases overall productivity or injectivity of the well. The specificity of the workflow is that it applies to crystalline rocks and includes an uncertainty and risk assessment framework.

II- Calibration study by using inverse problem method

The main challenge in these analyses is that the strength and stress profiles are unknown independently. Calibration of a geomechanical model on the observed borehole failure has been performed using data from the Basel Geothermal well BS-1 and inverse problem method (PEST: Parameter ESTimation software).

2.1- Parameters distribution before and after calibration

- We use breakout data from the BS1 borehole to develop and test our approach
- We calibrate on observations data (breakout width and length) between 3000 m and 3600 m depth
- We use Kirsch solution to compute breakout width by looking at the stress conditions at the borehole wall and comparing them to Mohr-Coulomb failure criteria
- The unknown stress profiles that need to be calibrated are the one for S_{Hmax} and S_{Hmin} . We consider that these profiles are simple linear functions of depth.

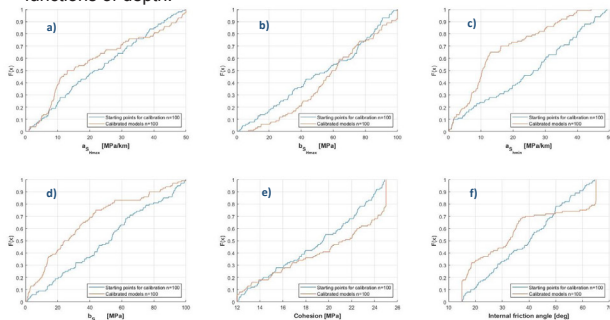


Figure 1. Distribution of initial and calibrated parameters (a) slope of S_{Hmax} , (b) intercept of S_{Hmax} , (c) slope of S_{Hmin} , (d) intercept of S_{Hmin} , (e) cohesion, (f) internal angle of friction for $n = 100$ starting points

2.2- Calibrated breakout width and length

The calibrated breakout width and length profiles for $n = 100$ starting points as well as the 25 observations are plotted below between 3000m and 3600m. Some of the curves fit the data well while some of them diverge for both breakout width and length.

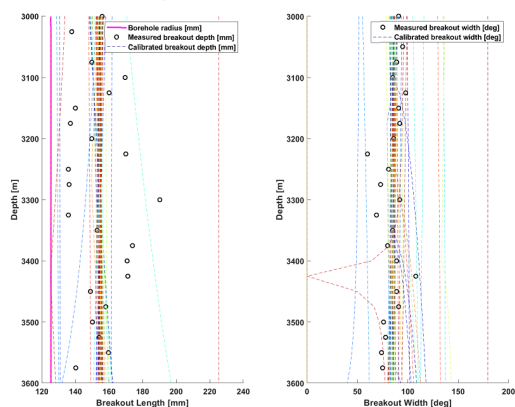


Figure 2. Left: Measured breakout penetration (black circles) and calibrated breakout penetration profiles (dashed lines) for $n = 100$ different starting points, right: Measured breakout width (black circles) and calibrated breakout width profiles (dashed lines) for $n = 100$ different starting points

2.3- Failure prediction results

We predict failure from 3.6km to 5km depth by calculating the breakout width and length based on previous calibrated models. At the end of the process, we keep only 15 calibrated models that predict well the failure.

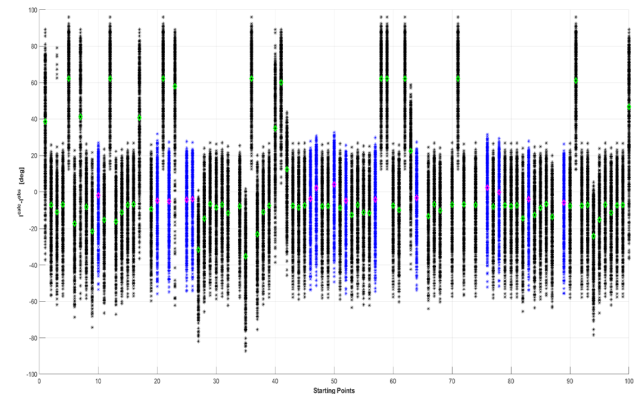


Figure 3. The difference $I(calc)-I(obs)$ Vs. the calibrated models. The models in blue predict the failure well from 3.6km to 5km as their median (in magenta) is close to zero.

2.4- Final «good» calibrated models

The final 15 calibrated models were used to calculate breakout width and length from 2.6km to 5km. Results are shown below:

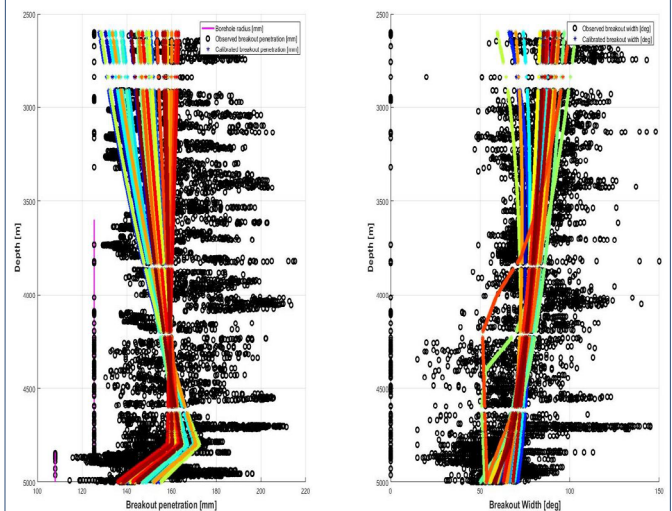


Figure 4. (left) calibrated breakout penetration (mm) and (right) calibrated breakout width from 2.6km to 5km

III- Conclusions

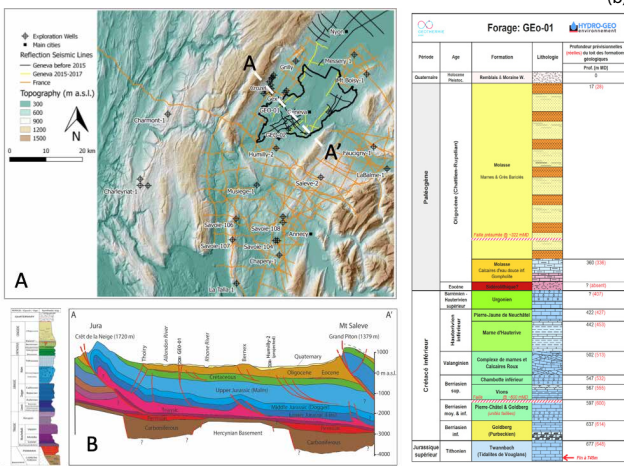
- Calibrated cohesion and friction angle tend to be high when using Mohr-Coulomb failure criterion
- Sensitivity to used failure criterion should be taken into consideration
- The calibrations are still not «perfect» and not unique but uncertainties should be quantified.
- Variability of the calibrated parameters should be integrated.

Application of Chemostratigraphy and petrology to characterize the Reservoirs of The Mesozoic sequence crossed by the Geo-01 well: potential for direct heat production and heat-storage.

Ferreira De Oliveira G.1, De Haller A. 1, Gugliemetti L. 1, Makhloufi Y. 1, Moscariello A.1.
1: University of Geneva – Earth Sciences Department. Rue des Maraichers 13, 1205 Geneva (Switzerland)
gustavo.ferreira@etu.unige.ch

SCCER-SoE
SWISS CONFERENCE CENTER FOR ENERGY RESEARCH
SUPPLY OF ELECTRICITY

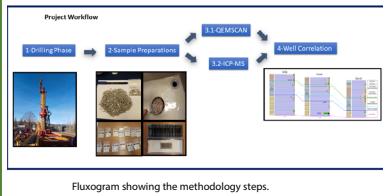
1. Introduction



The Satigny well is the first medium-depth exploration well of the Géothermie 2020 program. This pilot project will make it possible to specify the geothermal potential available and to confront the concrete realities on the subsurface. The purpose of Geo-01 is to explore the Mesozoic units and to identify and characterize the geological and hydrogeological conditions of the subsurface units. Geo-01 went through 407 meters of Tertiary Molasse, 241 meters of Cretaceous limestones and reached the Tithonian limestones at a final depth of 745 meters. Hot water was found at different depths. This water naturally rises to the surface at a temperature of 33 °C with a flow rate of more than 50 litres / second.

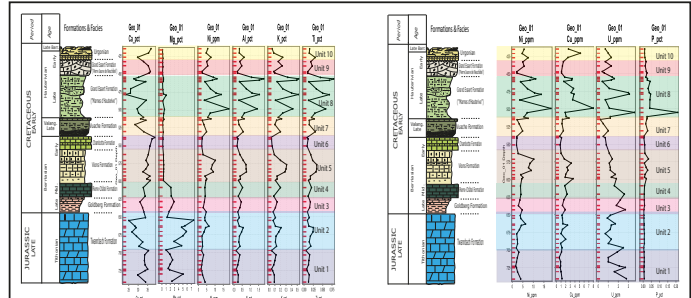
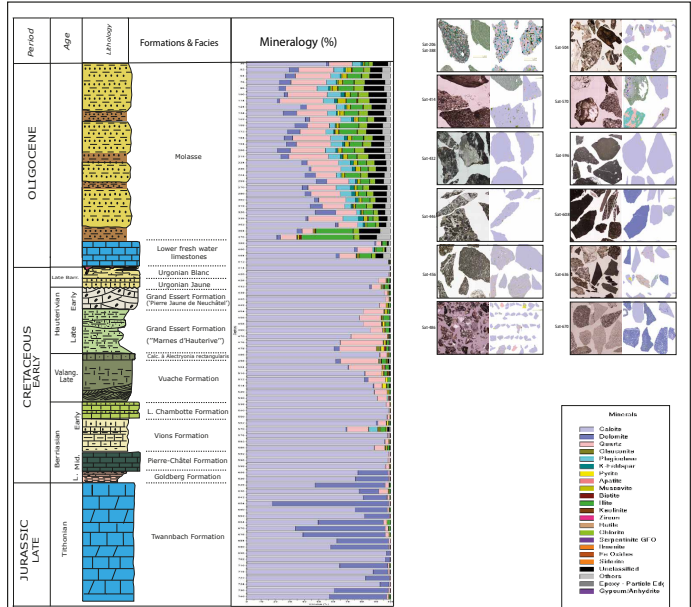
A) The Geneva Basin and surrounding region with location of main boreholes and 2D seismic lines acquired to date. The main wells used in this project (Geo-01, Crozet, Grilly, Humilly-2 and Thônex-1) are also indicated;
B) Simplified stratigraphic columns and NW-SE geological cross-section (AA') showing the principal stratigraphic and tectonic features of the GB (drawings modified from Moscariello et al., 2020)

2. Metodology

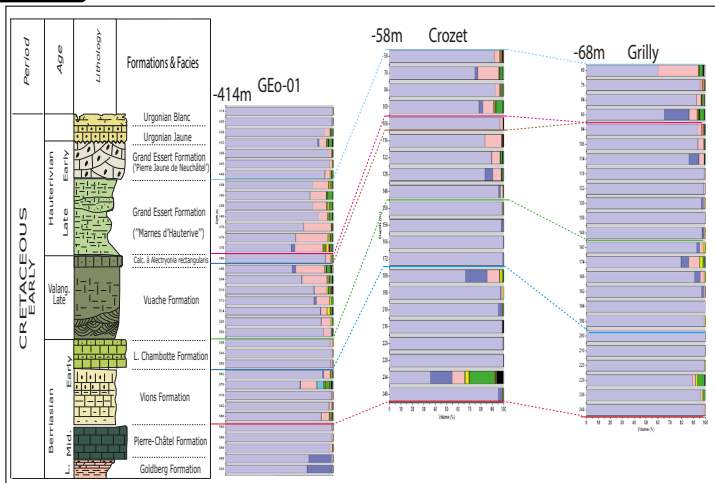
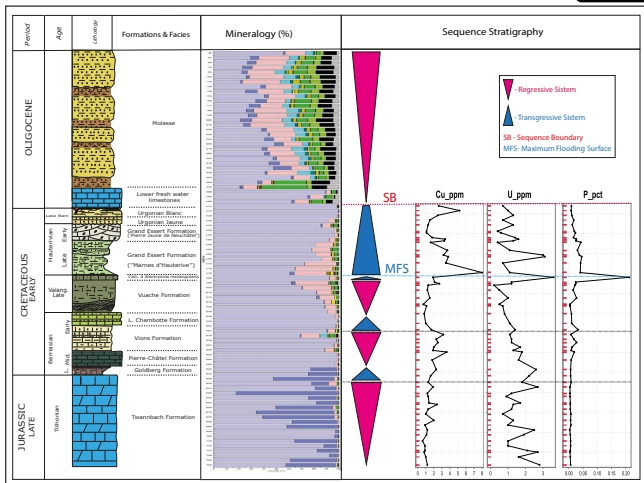


To realize this project several samples were provided by the Géothermie 2020 project. The cutting samples were taken during the Geo-01 drilling phase. A complete petrographic and mineralogical characterization has been done using QEMSCAN analysis and optical microscopy. This is aimed to have a better understanding of the composition and repartition of the sedimentary facies and to help correlate the stratigraphy of Geo-01 with other reference wells in the GGB (HU2; TH1; GRY1; CRO1).

3. Results



4. Discussion



5. Conclusions

Bibliography:
PGG (2011). Evaluation du potentiel géothermique du canton de Genève – Vol. 1: Rapport final. Technical report, Service cantonal de l'énergie-Service Industriels de Genève.
RUSILLON, Elme. Characterisation and rock typing of deep geothermal reservoirs in the Greater Geneva Basin (Switzerland & France). Université de Genève. www.geothermie2020.ch

GE RGBA GROUP
Geo Energy / Reservoir Geology
and Basin Analysis

- The geochemical and petrological analysis of the sedimentary sequences traversed by the Geo-01, Crozet and Grilly wells allows us to recognize and characterize the main sedimentary facies in the subsurface of the GGB.
- With the new data generated by this type of study it is possible to correlate wells present in the same geological context and to check the lateral continuity and thickness of the sedimentary packages along the basin.

Hydraulic Characterization of the Bedretto Underground Laboratory

Nima Gholizadeh Doonechaly^a, Nathan Dutler^b, Bernard Brixel^a, Marian Hertrich^a and Simon Loew^a

^aDepartment of Earth Sciences, ETH Zurich, CH-8092, Zurich

^bCentre for Hydrogeology and Geothermics, University of Neuchâtel, CH-2000, Neuchâtel

Introduction

Bedretto underground research laboratory in the Bedretto Adit of the Furka Base Tunnel (BUL) is a multi-disciplinary collaborative project of the Swiss Competence Centre for Supply of Energy. Completion and inauguration of this test facility operated by the Department of Earth Sciences at ETH was carried out on May 18, 2019. The first large scale experiments carried out in this lab are related to enhanced geothermal systems and will include drilling of a large number of long (250-300m) injection and monitoring boreholes. A hydrogeological model of the test volume is a fundamental component of this multi-disciplinary project and will be developed from a combination of measurements carried out during the drilling operations, and during a special characterization phase following the drilling phase. The long boreholes will also be monitored using pressure sensors over longer term after the hydraulic characterization phase. Prior to the main characterization phase of the project on the long boreholes, several short boreholes are already drilled in the BUL and used for preliminary analysis of the system.

Permeability Estimation

Based on the observed fracture map in the short boreholes, hydraulic characterization is carried out by packer testing of individual fractures to obtain the permeability value and water discharge (if any) from each individual fracture.

The permeability value measurement is carried out using pressure pulse test with applying a short pulse by injection at a high pressure and monitoring the transient pressure decline. The diffusivity equation is then used as a basis to estimate the fracture permeability value. The results for the pulse pressure testing of the single fracture at the depth of 20.7m at the SB1.1 borehole in BUL is presented in Figure 2. The packer interval's pressure is increased to 46.01bar over approximately 4 seconds. The interval's pressure was then monitored for a duration of 30 minutes while recovering towards formation pressure. The pressure decay into the interval containing the single fracture is presented in Figure 2.

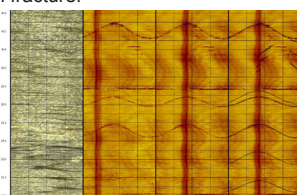


Figure 1: Selected interval of the OTV and ATV of wellbore SB1.1 before and after mini-fracture experiment.

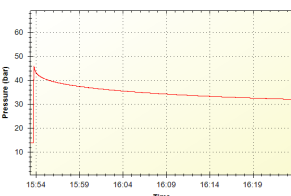


Figure 2: Pressure decline curve for the single fracture at the depth of 20.7m after applying a pressure pulse.

The analysis of the pressure decline curve is analysed using the curve fitting to analytical solution for diffusivity equation. Based on the obtained pressure data, and assumption of fracture aperture of 1µm, the fracture permeability is estimated as 5E-13 m². The flow rate from the borehole SB1.1 is also monitored and recorded at 0.12L/min.

Characterization of Long Boreholes

In the next phase of the experiment, the long boreholes (which are currently being drilled (Figure 3)) in the BUL will be analysed with a comprehensive hydro-geological analysis, including, flow measurement while drilling, heat dilution test, pulse test, cross hole test and tracer tests. After the hydraulic characterizations, the long boreholes will be equipped by a network of multi-disciplinary monitoring devices, such as microseismic, pressure, fiber-optics strain and temperature sensors so as to provide the required data for the design, execution and evaluation of the hydraulic stimulation.



Figure 3: Ongoing operation for drilling of the long boreholes in BUL.

Flow Measurement While Drilling

The initial estimate of the major flowing zones in the boreholes will be identified from the flow measurements during drilling (Figure 4). For this purpose, a side flow line is connected to the blowout preventer to directly measure the flow discharge from the borehole. The borehole flow is fully directed towards an electromagnetic flow meter and recorded continuously. Also several times a day, during the drilling breaks, borehole will be shut in and a pressure sensor is used to monitor the pressure build up within the borehole. Such tests, gives us first hand estimate of the flowing intervals within a boreholes as well as an estimate of the permeability of corresponding intervals.



Figure 4: Flow measurement during drilling operation.

Fluid Flow Logging using Heat Dilution Test

The major flowing zones (fractures) of boreholes will be qualitatively identified using heat dissipation-tests. Hybrid heating cable and fiber optic distributed temperature sensing (FO-DTS) will be implemented in the corresponding boreholes, individually, to measure the wellbores' response to artificially induced temperature disturbances using a heating cable. The heating cable will be used to heat up the wellbore to a temperature of ~20°C above the formation temperature in a relatively short period of time. After heating the borehole, the borehole fluid temperature profile will be continuously monitored with the installed FO cable while the wellbore can flow freely at natural conditions. The transient temperature profile will be continuously monitored until stabilized condition is reached. Then the obtained data will be analyzed to identify the flowing zones along the borehole length. The above-mentioned procedure will be repeated for all boreholes.

Hydraulic Tomography

After identifying the major flowing zones in the boreholes (identified from heat dilution test), packer testing will be carried out to test the permeability of the transmissive fractures in corresponding flow zones. Then Hydraulic tomography will be carried out to reconstruct the heterogeneity and directional properties of the system. For this purpose, the cross hole well testing will be carried out followed by injecting three different fluorescent dye tracers in transmissive intervals. The inversion will be carried out using both numerical and analytical techniques.

Discussion & Conclusions

The preliminary results from the short boreholes shows the influence of the hydraulic fractures on creating the connected flow path in the borehole. The results also show shows the heterogenous nature of the hydraulic properties of the system, even within the same well. Therefore, large scale characterization using tracer and cross hole test in long boreholes play major role in understanding the hydraulic characteristics of the system.

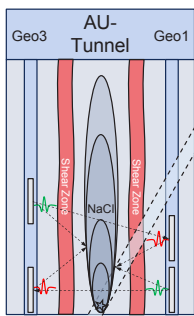
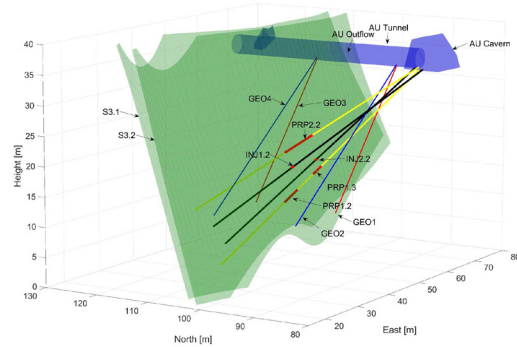
References

- Cooper Jr, H.H., Bredehoeft, J.D. and Papadopoulos, I.S., 1967. Response of a finite-diameter well to an instantaneous charge of water. *Water Resources Research*, 3(1), pp.263-269.
- Papadopoulos, S.S., Bredehoeft, J.D. and Cooper Jr, H.H., 1973. On the analysis of 'slug test' data. *Water Resources Research*, 9(4), pp.1087-1089.
- Masset, O. and Loew, S., 2013. Quantitative hydraulic analysis of pre-drillings and inflows to the Gotthard Base Tunnel (Sedrun Lot, Switzerland). *Engineering geology*, 164, pp.50-66.
- Renard, P., 2017. Hytool: an open source matlab toolbox for the interpretation of hydraulic tests using analytical solutions. *J. Open Source Software*, 2(19), p.441.
- <https://escholarship.org/uc/item/03q0365v>
- Jalali, M., Klepikova, M., Doetsch, J., Krietsch, H., Brixel, B., Dutler, N., Gischig, V. and Amann, F., 2018, November. A Multi-Scale Approach to Identify and Characterize the Preferential Flow Paths of a Fractured Crystalline Rock. In *2nd International Discrete Fracture Network Engineering Conference*. American Rock Mechanics Association.

Monitoring and Flow Path Reconstruction of Saline Tracer Tests with GPR

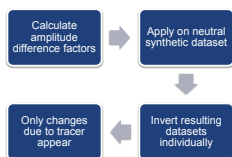
 Peter-Lasse Giertzuch¹, Joseph Doetsch¹, Mohammadreza Jalali², Alexis Shakas¹, Cédric Schmelzbach¹, Hansruedi Maurer¹
¹Department of Earth Sciences, ETH Zurich, Switzerland; ²RWTH Aachen University, Chair of Engineering Geology and Hydrogeology, Germany

1 Introduction

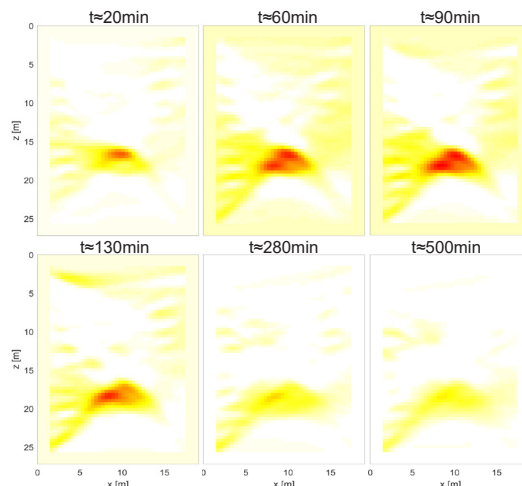


In two experiments at the Grimsel Test Site (GTS) in Switzerland, 100 L and 200 L of salt water were injected at a rate of 2 L/min in INJ2 in between the S3 shear zones, and time-lapse Ground Penetrating Radar (GPR) reflection data were recorded in GEO3 and GEO1 in the respective tests. Simultaneously, transmission data was recorded by using a 4-channel system and two 250 MHz borehole antenna sets. The temporal resolutions were ~10 min and ~30 min for the reflection and transmission acquisition, respectively. The upper figure shows the GTS with INJ, GEO and PRP boreholes, as well as the S3 shear zones. On the left the GPR survey schematic is shown.

2 Difference Attenuation Tomography

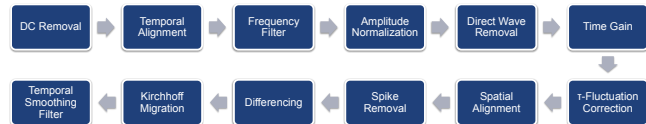


The transmission data is analyzed by a Difference Attenuation Approach. This approach allows to invert for changes due to the tracer only, disregarding all geological information in the GPR data (top). The time-lapse datasets are inverted individually and show clearly the tracer injection, build up and signal decrease in the tomography plane over time.



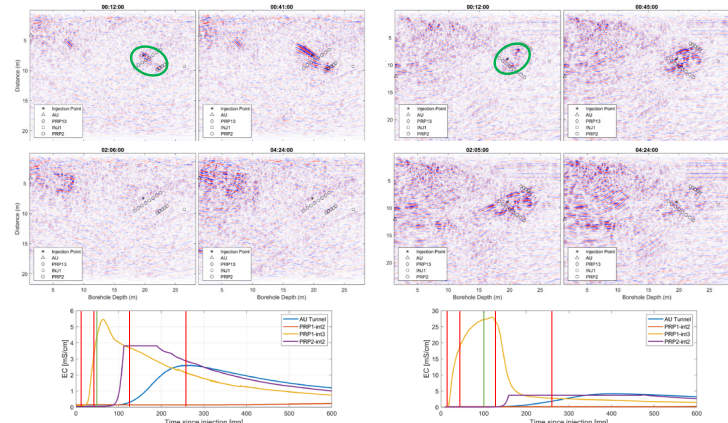
The tracer appears to cross the tomography plane only once near the injection point and is not resolved towards shallower borehole depths.

3 Difference Reflection Imaging



The concept of Difference Reflection Imaging relies on subtracting a reference profile that was recorded prior to tracer injection from all of the following time-lapse monitoring profiles. Only changes due to the salt tracer remain. The necessary processing steps are shown above. Special attention needed the fluctuation of the sampling rate during data acquisition. The developed correction is based on resampling and cross-correlation to reconstruct compatible waveforms. The process is described in [1].

Below: Four differenced profiles from the two experiments at different times after tracer injection and measured breakthrough curves in different borehole intervals. Symbols represent the calculated reflection positions of the different borehole intervals. The tracer first appears around the injection point, appears to split up and propagates towards PRP13 and the AU tunnel outflow. The tracer reflection are in good accordance with the measured breakthrough curves at the different positions. Note that the PRP2 curve is clipped.

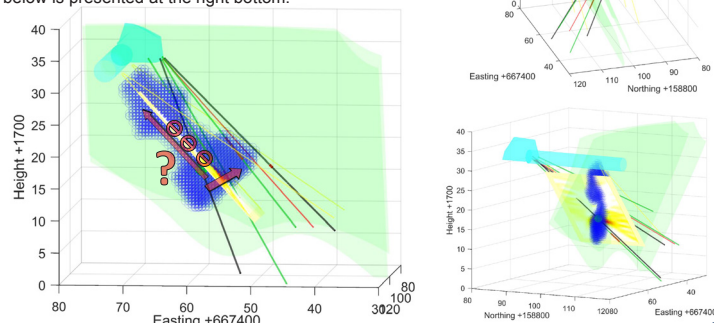


[1]: Giertzuch et al. (in review), GEOPHYSICS

4 3D Flow Path Reconstruction

Single-hole reflection GPR data does not allow for actual localization, as the antennas show a radial symmetry, but this can be overcome by combining the two datasets. After migration, a tube shaped form contains the possible reflection locations (right top). The data from the GEO1 and the GEO3 surveys are combined by calculating the intersections of those shapes and thereby allow for a 3D localization of the tracer flow path in blue (right middle).

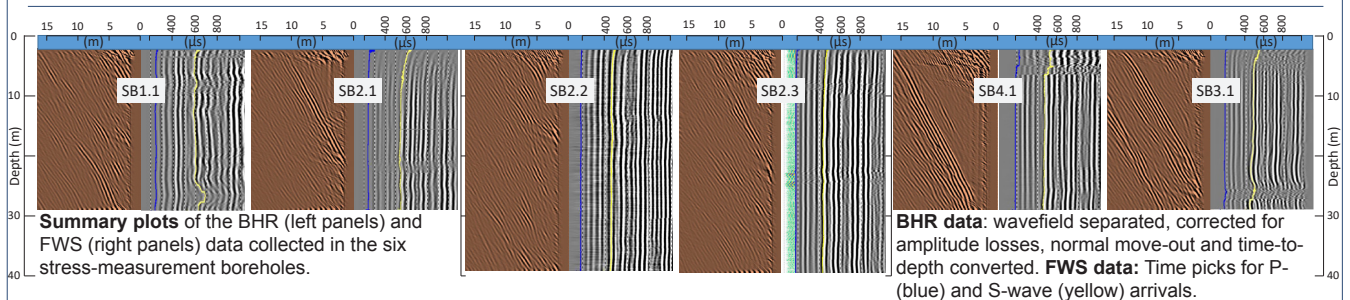
Combined with the difference attenuation results it is possible to further constrain the flowpath (bottom). The tracer splits close to the injection point, one part propagates through the tomography plane towards PRP13, the other part seems to stay below the plane propagating towards the AU outflow. The view from below is presented at the right bottom.



Borehole radar and full waveform sonic measurements of the Bedretto stress-measurement boreholes

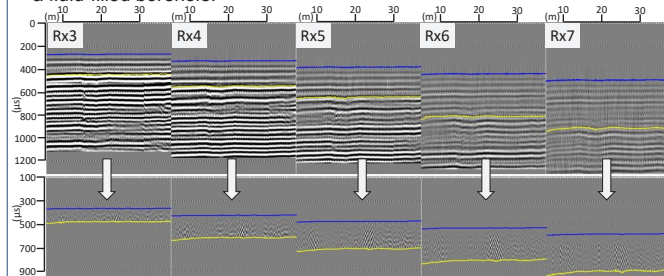
Andrew Greenwood, Eva Caspari, Ludovic Baron and Klaus Holliger.

Abstract: High-quality and high-resolution wireline logging has been completed in the Bedretto Underground Laboratory stress-measurement boreholes (SB) to assist determination of the local stress field and characterise the rock mass. Here we present preliminary results of borehole radar (BHR) and full-waveform sonic (FWS) data with particular emphasis on the method's ability to locate and map hydraulically open fractures.

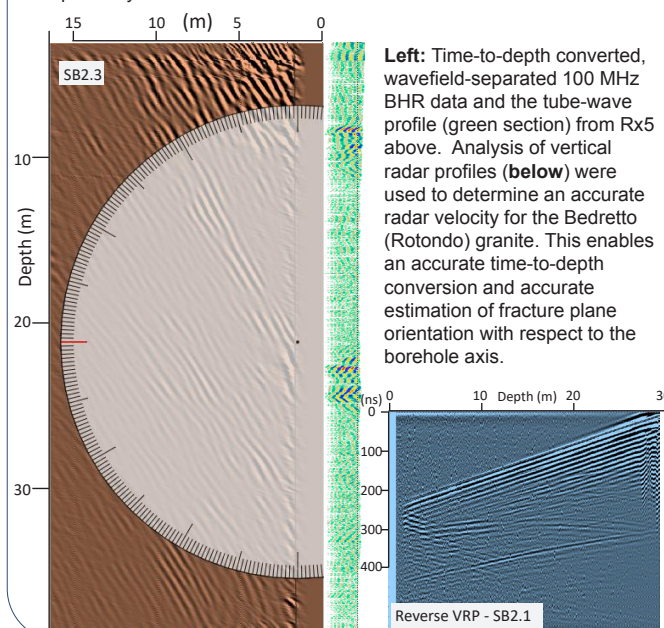


Fracture detection and mapping

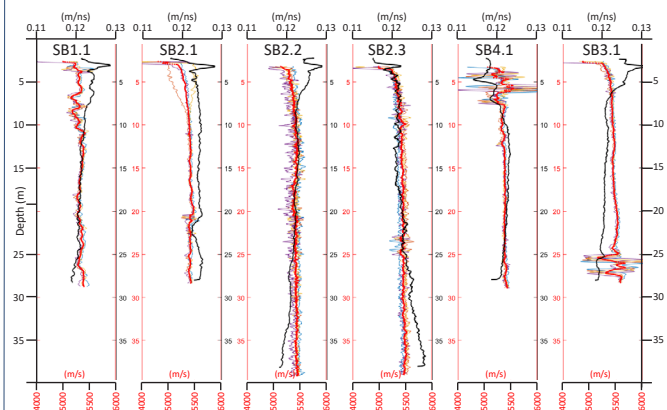
Fluid-filled fractures within crystalline rocks can be detected by their high-contrasting conductivity in BHR data, and in borehole acoustic methods, such as FWS, when a hydraulically open fracture intersects a fluid-filled borehole.



Bottom: Data after removal of head-wave modes which reveals tube-waves generated at hydraulically open fractures by passing acoustic waves. These are observed as chevrons within the wavefield-separated profiles. Blue and yellow lines are P- and S-wave arrival travel-times, respectively.



Velocity comparison



Summary and outlook

We have collected high-quality full wave form sonic and borehole radar data in the six SB boreholes. This combination accurately locates open fractures by identifying tube-waves and infers the orientation and extent of the fracture plane away from the borehole.

It is possible to determine fracture compliance from the amplitude ratio between the onset acoustic wave and the corresponding generated tube wave. We intend to modify the inversion scheme of Hunziker (2019) to invert for fracture compliance from multi-receiver FWS data. Having multiple receivers allows for higher precision estimation of acoustic velocities and attenuation, and allows for a more robust inversion due to the additional offset tube-wave-profiles.

Reference:

Hunziker, J., A. Greenwood, S. Minato, N. Barbosa, E. Caspari and K. Holliger., 2019. Bayesian Full-Waveform Tube-Wave Inversion for Effective Hydraulic Fracture Aperture and Mechanical Fracture Compliance. 81st EAGE Conference and Exhibition, London, 2019,

Acknowledgement:

We thank the BULG team for their support.

Geochemical Characterization of Geothermal Waters Circulation in Carbonatic Geothermal Reservoirs of the Geneva Basin (GB)

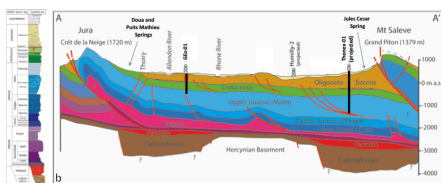
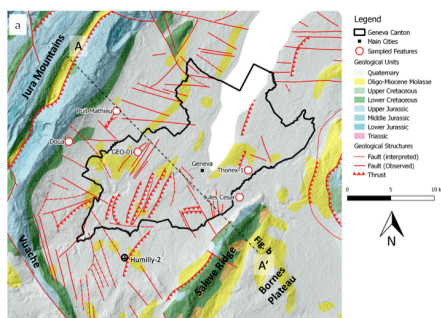
Guglielmetti L. *, Eichinger F. **, Moscariello A. *,

This study focuses on the interpretation of geochemical data collected at springs and at two deep geothermal exploration wells located on the edges and within the Geneva Basin (GB Canton of Geneva, Switzerland).

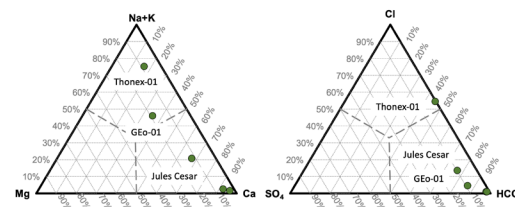
The sampling sites have been selected across one North-South trending sections following the main groundwater flow from the recharge zone to the deep geothermal reservoirs in the Mesozoic carbonatic units.

These formations have been drilled by two geothermal exploration wells; the 745 m deep GEO-01 well, where water with a temperature of 34°C and an artesian flow rate of 50l/s is encountered, and at the 2530 m deep Thonex-01 well, which produces app. 0.1 l/s by artesian flow at reservoir temperature of 80°C.

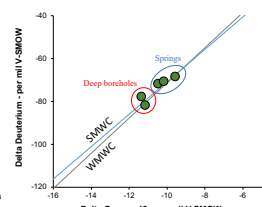
Major ions, trace elements, stable isotopes of Oxygen and Hydrogen, Tritium, Sulphur and Carbon isotopes as well as noble gas samples have been collected and analysed. The analyses aim at characterizing the fluid circulation in terms of recharge zone, origin of the water, mean residence times, reservoir temperature, and water-rock interactions.



RESULTS



Ternary plots of the analysed samples



Stable isotopes of Oxygen and Hydrogen showing the meteoric origin of the sampled waters

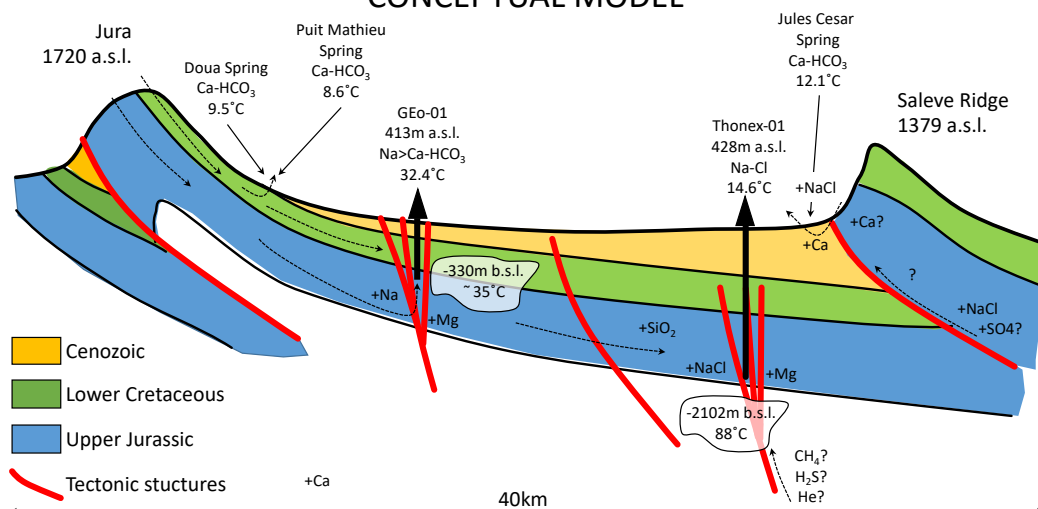
| | Puits Mathieu | Doua Spring | GEO-01 Well | Thonex-01 Well (bottomhole at 428m) | Jules Cesar Spring |
|------------------|---------------|-------------|-------------|-------------------------------------|--------------------|
| Temperature | 8.6 | 9.5 | 29.8 | 14.6 | 88.0 |
| pH | 7.5 | 7.5 | 7.5 | 7.7 | 7.9 |
| Calcite | -0.024 | -0.075 | -0.072 | 0.246 | -0.011 |
| Aragonite | -0.209 | -0.229 | -0.215 | 0.191 | -0.164 |
| Dolomite | -1.258 | -1.495 | -0.075 | 0.514 | 1.931 |
| Gypsum | -3.041 | -3.025 | -2.611 | -4.150 | -4.162 |
| Anhydrite | -3.534 | -3.509 | -2.910 | -4.626 | -3.859 |
| Amorphous Silica | -2.111 | -1.818 | -1.255 | -0.803 | -1.366 |
| Chalcedony | -1.213 | -0.923 | -0.417 | 0.089 | -0.702 |
| Quartz | -0.730 | -0.443 | 0.010 | 0.568 | -0.435 |

Elevation estimation based on $\delta^2\text{H}$ and $\delta^{18}\text{O}$ isotopes

| Sample Name | Na-K-Ca | Measured Temperature |
|--------------------|---------|----------------------|
| Puits Mathieu | - | - |
| Source de la Doua | - | - |
| GEO-01 Well | 36 | 34 |
| Thonex-01 Well | 84 | 88 |
| Source Jules Cesar | 21 | - |

Reservoir temperature (°C) estimated by Na-K-Ca and measured after drilling

CONCEPTUAL MODEL



CONCLUSIONS: The interpretations show that the geothermal waters have a meteoric origin with the main recharge zone being located in the Jura Mountains towards the North.

The infiltration is dominated by secondary porosity controlled by intense fracture conditions.

Infiltrating water circulates in the Mesozoic Units and the groundwater flow direction is controlled by the geometry of these formations, which gently dip towards south with a 3° average dip.

Fracture zones associated to sub-vertical strike-slip faults represent the main corridors where waters as well as hydrocarbons and dissolved gas rise towards the surface. Moreover, the highly porous and permeable karstified horizons at the Lower Cretaceous level and the reef complex in the Upper Jurassic represent very promising potential geothermal reservoirs across the whole Geneva Canton for heat production with temperatures ranging from about 30°C to more than 110°C.

*Department of Earth Sciences, University of Geneva. Rue des maraichers 13, 1205 Geneva (Switzerland)

**Hydroisotop GmbH. Woelkstr. 9, D-85301 Schweitenkirchen (Germany)

luca.guglielmetti@unige.ch

ACKNOWLEDGEMENTS

The authors would like to thank Services Industriels de Genève for funding this research and providing access to the well sites, and HydroGeo Environnement Sarl for the fruitful support and dialogues in selecting the sampling sites

Bayesian inversion of tube waves to estimate fracture aperture and compliance: Application to a real dataset

Jürg Hunziker, Andrew Greenwood, Shohei Minato, Nicolas Barbosa, Eva Caspari and Klaus Holliger

Introduction

We propose to estimate the effective hydraulic aperture of fractures as well as their mechanical compliance, through a Bayesian full-waveform inversion of tube waves. Tube waves are created when a seismic body wave encounters a fluid-filled fracture which is connected to a borehole. When such a fracture is deformed by the passing body wave, fluid is squeezed into the borehole. This creates an acoustic disturbance known as a tube wave, which propagates along the borehole wall. Usually, tube waves are considered as noise in the processing of vertical seismic profiling (VSP) data, but here we profit from the fact that the characteristics of tube waves depend on the displaced fluid volume to infer the effective hydraulic aperture and the mechanical compliance of fractures.

Method

Considering the small parameter space and the strong non-linearity of the inverse problem, we chose to use a stochastic instead of a deterministic inversion approach. This has the following advantages:

- Our Bayesian inversion does not infer only one single model that explains the data, but rather an entire ensemble allowing to sample the posterior probability density function and, thus, providing a measure of uncertainty.
- The algorithm is able to leave local minima. It is therefore sufficient to draw random models from the prior probability density function to initialize the inversion.

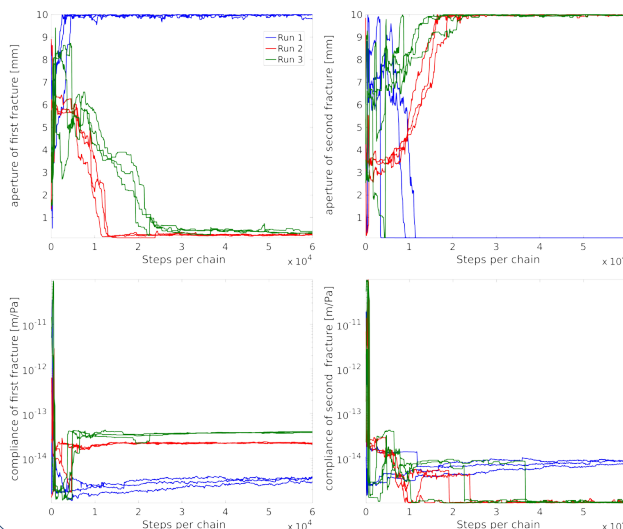
We sample the posterior probability density function using the DREAM(ZS) algorithm (ter Braak and Vrugt, 2008; Laloy and Vrugt, 2012), which is a Markov chain Monte Carlo (MCMC) approach using multiple interacting chains and a database of past models for fast convergence.

As a forward solver, to simulate the tube-wave data during the inversion process, we use the semi-analytic algorithm of Minato and Ghose (2017) and Minato et al. (2017) with the following extensions:

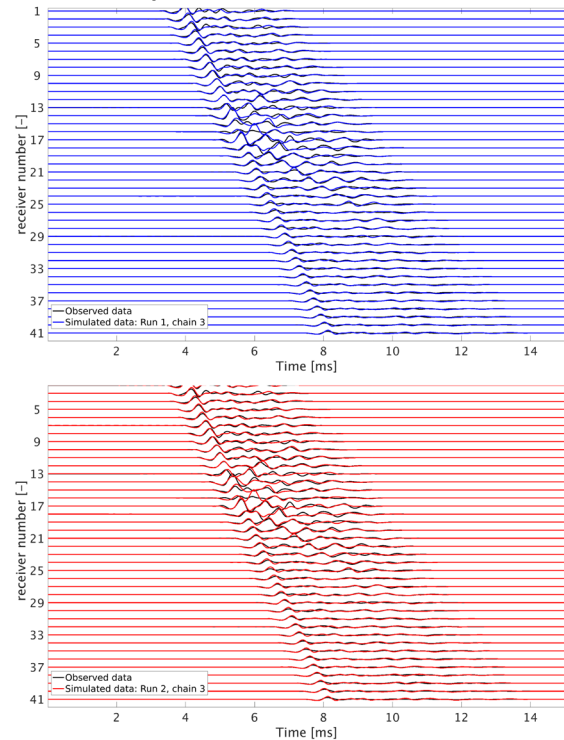
- Geometrical spreading for body waves
- Transmission losses of body waves across fractures
- Variable source-depth to accommodate velocity changes above the borehole section under consideration
- Separate effective isotropic shear moduli for the body waves and for the tube waves to take anisotropy into account

Results: modelspace

We apply our inversion algorithm to zero-offset VSP data from the Grimsel test site in Switzerland. The inversion was run three times with each run consisting of three interactive Markov chains. The development of the estimates of the aperture and mechanical compliance for two fractures, which are separated from each other by only 0.4 m vertical distance, are plotted below.



Results: dataspace



These results show that our Bayesian inversion approach discovered two equally probable models: Either the first fracture has a large aperture and a relatively small compliance while the second fracture has a small aperture and a relatively large compliance (as discovered by run 1) or vice versa (run 2 and 3).

Conclusions

- We have developed a stochastic full-waveform inversion approach for tube waves and applied it to a field dataset from the Grimsel test site in Switzerland. The method allows to explain the data well.
- Our Bayesian tube-wave inversion is able to determine that one of the two fractures has a larger aperture than the other. The identification of these two equally probable models nicely illustrates one of the key advantages of Bayesian inversion compared to a deterministic approach, which would have converged only to one of these solutions.
- Optical televiewer data and a study based on the attenuation analysis of full-waveform sonic log data (Barbosa et al., 2019) support the solution proposed by the 2nd and 3rd run.

References

- Barbosa, N. D., Caspari, E., Rubino, J. G., Greenwood, A., Baron, L. and Holliger, K. [2019] Estimation of fracture compliance from attenuation and velocity analysis of full-waveform sonic log data, *Journal of Geophysical Research: Solid Earth*, 124, 2738-2761.
- ter Braak, C.J.F. and Vrugt, J.A. [2008] Differential evolution Markov Chain with snooker updater and fewer chains. *Statistics and Computing*, 18(4), 435-446.
- Laloy, E. and Vrugt, J.A. [2012] High-dimensional posterior exploration of hydrologic models using multiple-try DREAM (ZS) and high-performance computing. *Water Resources Research*, 48, W01526.
- Minato, S. and Ghose, R. [2017] Low-frequency guided waves in a fluid-filled borehole: Simultaneous effects of generation and scattering due to multiple fractures. *Journal of Applied Physics*, 121(10), 104902.
- Minato, S., Ghose, R., Tsuji, T., Ikeda, M. and Onishi, K. [2017] Hydraulic properties of closely spaced dipping open fractures intersecting a fluid-filled borehole derived from tube wave generation and scattering. *Journal of Geophysical Research: Solid Earth*, 122, 8003-8020.

In-situ stress estimation from fault slip triggered during fluid injection

Maria Kakurina¹, Yves Guglielmi², Christophe Nussbaum³ and Benoît Valley¹

(1)University of Neuchâtel, CHYN, Neuchâtel, Switzerland, (2) Lawrence Berkeley National Laboratory, Berkeley CA, United States, (3) Swisstopo, Wabern, Switzerland

Introduction

Standard **in situ stress measurement** methods using fluid injection in deep boreholes are based on the analyses of pressure, flowrate and pre- and post-injection fracture mapping. Here we apply a **new methodology** to improve the estimation of the in situ stress by adding the record of **three-dimensional (3D) displacement** in the pressured interval measured continuously during the injection. We use the displacement-flowrate-pressure data from a **fault reactivation** experiments conducted in shale rocks at the Mont Terri rock laboratory, Switzerland. The experiment consisted in fluid injections into the fault damage zone in order to reactivate the fault planes and to measure the slip during the injection. The experiment protocol followed the step-rate injection method for fracture in situ properties (SIMFIP) developed by Guglielmi et al. (2013).

Input data

Stress orientations and magnitudes are estimated using the data of (Table 1):

- 1) Geology of the injected interval
- 2) Measured slip orientation (Figure 1)
- 3) Normal stress (σ_n) on the reactivated fracture (ISIP)
- 4) Vertical stress (σ_v) on the reactivated fracture ($\sigma_v = \sum_{i=1}^n \rho_i g \Delta z$)

Table 1. Summary of the input data

| Potentially activated fractures | | Slip direction | | Projected slip | | Normal stress, MPa | Vertical stress, MPa |
|---------------------------------|-----------|----------------|-----------|----------------|-----------|--------------------|----------------------|
| Dip Direction | Dip Angle | Dip Direction | Dip Angle | Dip Direction | Dip Angle | | |
| 130 | 55 | 75 | 25 | 75 | 39 | 4.4±0.2 | 7.2±0.2 |
| 130 | 46 | | | | 31 | | |
| 131 | 65 | | | | 50 | | |
| 130 | 37 | | | | 23 | | |

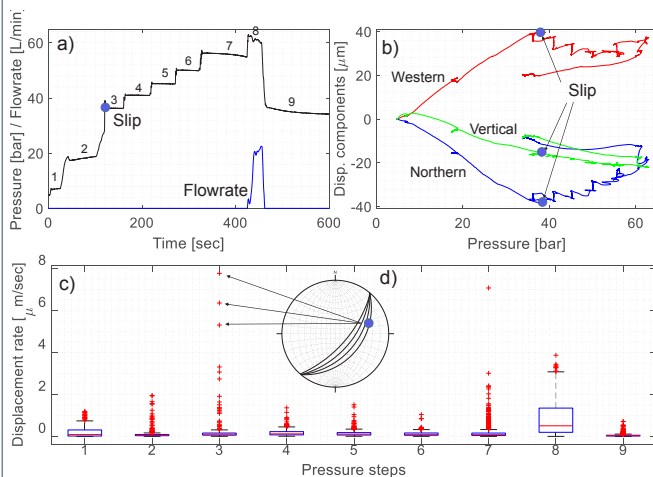


Figure 1. a) Pressure, flowrate and b) 3 components of displacement monitored during the step-rate test and indication when slip occurs, c) Box plot of displacement rate at each pressure step used to identify slip events, d) Stereoplot with the slip direction of identified slip events and fractures in the interval.

References

Guglielmi, Y., Cappa, F., Lançon, H., Janowczyk, J. B., Rutqvist, J., Tsang, C. F., & Wang, J. S. Y. (2013). ISRM suggested method for step-rate injection method for fracture in-situ properties (SIMFIP): Using a 3-components borehole deformation sensor. In The ISRM Suggested Methods for Rock Characterization, Testing and Monitoring: 2007-2014 (pp. 179-186). Springer International Publishing.

Protocol of estimation the complete stress tensor

(1) Grid search over all possible reduced stress tensor (orientation and stress ratio R) in order to identify the ones compatible with observed slip orientation (good FIT value) (Figure 2)

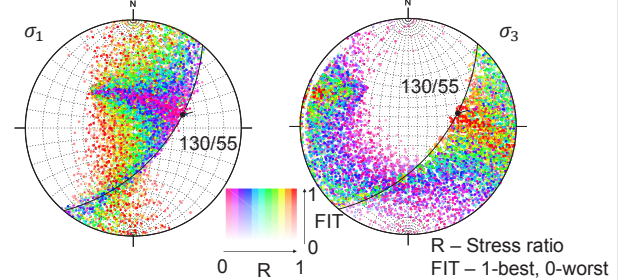


Figure 2. All possible stress combinations and their fit to the fracture slip. Example: fracture oriented 130°/55°

(2) Sorting of the possible reduced stress tensor keeping only those with a FIT > 90% , i.e. allowing for a max misfit angle between measured and calculated slip of 5.7° or less.

(3) Calculating absolute principal stress magnitude values $\sigma_1, \sigma_2, \sigma_3$ by considering the accepted reduced stress tensor and estimations of the vertical and fracture normal stress. This is done by solving the following system of equations:

$$\begin{cases} R = \frac{\sigma_2 - \sigma_3}{\sigma_1 - \sigma_3} \\ \sigma_n = l_1^2 \sigma_1 + m_1^2 \sigma_2 + n_1^2 \sigma_3 \\ \sigma_v = l_2^2 \sigma_1 + m_2^2 \sigma_2 + n_2^2 \sigma_3 \end{cases}$$

where l, m and n are the direction cosines of the normal of the fracture with respect to the principal stress axes

(4) Reducing the number of possible solutions by insuring that only solutions showing high slip tendency on the considered fracture are kept and insuring acceptable bound on the principal stress magnitudes ($\sigma_1, \sigma_2, \sigma_3 > 1.5$ MPa and $\sigma_1, \sigma_2, \sigma_3 < 8$ MPa) (Figure 3)

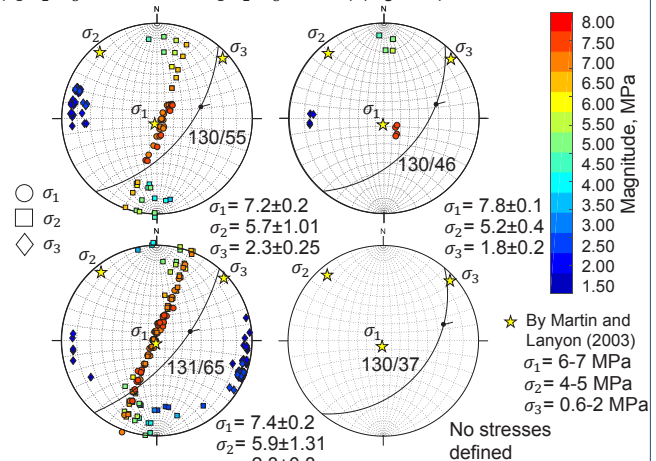


Figure 3. Orientations and magnitudes of the in situ stresses for potentially activated fractures

Conclusions


- The presented methodology allow estimating the full stress tensor from a single set of fracture activation measurements. Some uncertainties remains concerning what exact fracture is activated but this doesn't affect the robustness of the stress estimation.
- Estimation of the stress orientation and magnitudes is consistent with the state of stress, estimated in Mont Terri by Martin and Lanyon (2003):

Rock mechanics properties for fractured limestone hydrothermal system

Morgane Koumrouyan, Reza Sohrabi, Benoît Valley

Centre for Hydrogeology and Geothermics (CHYN), University of Neuchâtel, Switzerland
 morgane.koumrouyan@unine.ch

Supported by:

 Schweizerische Eidgenossenschaft
 Confederazione Svizzera
 Confederaziun Svizra
 Swiss Confederation
 Innosuisse – Swiss Innovation Agency




Motivation

This research aims at constraining the geomechanical properties of a fractured limestone hydrothermal system in the Geneva basin (Switzerland). This region is characterised by strike-slip and thrust faults [1] that increase locally the permeability. These structures are targeted by geothermal projects. We analyse logging data collected during drilling operations, especially optical and acoustic televiwers, and full-waveform sonic data. The study focusses on the assessment of fracture distribution, mechanical characteristics and stress state of the limestone surrounding the exploration well Géo-01.

Methods

Wellbore images analyses

We identify the fractures (Figure 1) and determine their orientation, dip angle and aperture based on the optical and acoustic images of the well. Transit time measurements recorded by the acoustic tool are converted into radius to analyse the well shape.

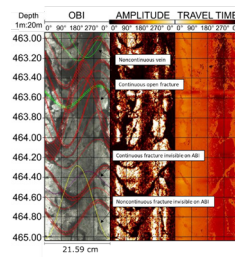


Figure 1: Fractures displayed on optical and acoustic televiwers.

Rock mechanical properties

From the full-waveform sonic data, we extract estimations of the P-wave and S-wave velocities of the formation using a semblance analysis [2]. We combine with density log to calculate the Poisson's ratio (ν), and the Young's modulus (E) of the rock assuming a linear elastic and isotropic rock:

$$\nu = \frac{V_p^2 - 2V_s^2}{2(V_p^2 - V_s^2)} \quad ; \quad E = \frac{\rho V_s^2 (3V_p^2 - 4V_s^2)}{V_p^2 - V_s^2} \quad \text{Eq. 1}$$

Stress state

An estimation of the expected vertical stress magnitude is obtained by the integration of density data (Eq. 2). Bounds on allowable horizontal stresses is calculate by considering purely frictional stability (Eq. 3) for a coefficient of friction μ of 0.6 and 1.0 (Figure 2).

$$S_v = \int_0^z \rho(z) g dz \quad \text{Eq. 2}$$

$$\frac{\sigma_1 - P_p}{\sigma_3 - P_p} = [(\mu^2 + 1)^2 + \mu]^2 \quad \text{Eq. 3}$$

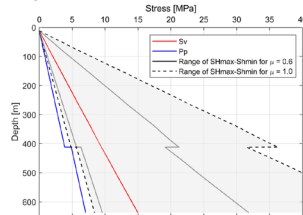


Figure 2: Ranges of SHmax, Shmin, Sv and Pore pressure expected in the well.

We further constrain the horizontal stress magnitudes by estimating the impact of stiffness contrast between the various layers of our sedimentary column determined from the sonic logging data. We apply a displacement boundary mimicking tectonic loading to a finite element stress model consisting of 14 layers. Stiffer layers attract larger stress magnitude (Figure 3).

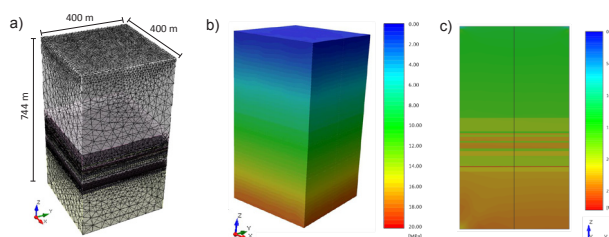


Figure 3: a) Mesh Geometry, b) vertical stress magnitude and c) SHmax magnitude variations induced by displacement.

Fracture slip tendency

Having measurements for the fractures orientations and an estimate of the in-situ stress state, we can compute the slip tendency (T_s) on the fractures defined as the ratio of shear (τ) to normal tractions (σ_n) resolved on the fracture planes (Eq. 4). Fractures with larger slip tendency are closer to shear failure [3] and are often considered as the active flow paths in the fractured rock mass [4].

$$T_s = \frac{\tau}{\sigma_n} \quad \text{Eq. 4}$$

Results

A synthesis of our stress and fracture data are presented in Fig. 4. An important clockwise rotation of the fracture orientation is observed according to depth (Figure 4). Between 460.0 and 480.0 meters deep, steeper dip angles and highly fractured carbonates highlight interaction of the wellbore with a faulted zone. It induces local stress heterogeneities in the vicinity of the well and stimulate the development of fractured networks.

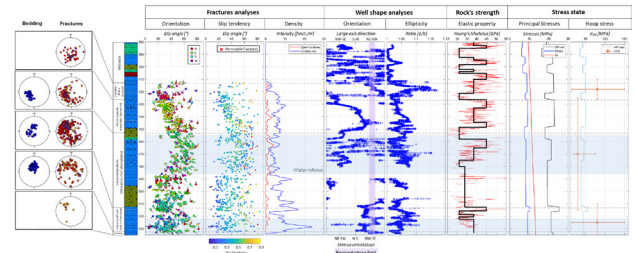


Figure 4: Fractures characterisation, borehole shape analyses, rock's strength evaluation and stress state estimation along the Géo-01 borehole.

Sections characterised by water inflows present critically stressed open fractures. The latter might enhance the permeability of the fracture limestone reservoir and significantly contribute to fluid circulations by creating important hydraulic conduits.

According to shale content variations, large stiffness contrasts appear at stratigraphic limits and could be responsible for important variations of the in situ stress magnitude and of the fracture orientation.

Conclusions

These rock physical analyses highlight that the presence of a faulted zone crossing the borehole related to a flower structure in a strike-slip fault oriented NNW-SSE contributes significantly to water inflows. Contrasting Young's modulus values are noticed along the well, influencing the stress accumulation into stiffer layers. The assessment of fracture distribution and rock mechanical properties provide thus good characterisation of the rocks surrounding a geothermal borehole.

Acknowledgements

This work is developed in collaboration with the Industrial Services of Geneva (SIG) and HydroGéo Environnement SA. It takes part in the framework of the European Project HEATSTORE (170153-4401) under the GEOTHERMICA-ERA NET Grant (N° 731117) supported by the the European Commission, RVO (the Netherlands), DETEC (Switzerland), FZJ-PtJ (Germany), ADEME (France), EUDP (Denmark), Rannis (Iceland), VEA (Belgium), FRCT (Portugal), and MINECO (Spain).

References

- [1] Clerc, N., Rusillon, E., Moscardelli, A., Renard, P., Paolacci, S., and Meyer, M. (2015). Detailed Structural and Reservoir Rock Typing Characterization of the Greater Geneva Basin, Switzerland for Geothermal Resource Assessment, Proceedings World Geothermal Congress 2015, Melbourne, Australia.
- [2] Valley, B., Bewick, R. P., and Hudson, R. (2011). Rock and rock mass characterization for deep mining using sonic data. In 45th US Rock Mechanics/Geomechanics Symposium. American Rock Mechanics Association.
- [3] Morris, A., Ferrill, D.A., Brent Henderson, D.B. (1996). Slip-tendency analysis and fault reactivation. *Geology* 24, 275.
- [4] Barton, CA, MD Zoback, and D Moos. (1995). Fluid Flow along Potentially Active Faults in Crystalline Rock. *Geology* 23 (8): 683–86.

Determine fault criticality using seismic monitoring and fluid pressure analysis

Léa Perrochet, Giona Preisig, Benoît Valley

Centre for Hydrogeology and Geothermics (CHYN), University of Neuchâtel

Setting, Motivations & Objectives

Better understanding fault criticality, the proximity of a fault to shear failure, is of primary interest when planning underground projects. Stress perturbations in the surroundings of a critically stressed fault, resulting from human activities, can affect the fault's stability - and eventually lead to a forced interruption of projects due to seismic risk.

Changes in the stress state also occur naturally. It has been observed [1] that in karstic regions, an increase in groundwater pressure following significant recharge (precipitations and/or seasonal snowmelt) can result in a fault re-activation, inducing microseismicity.

The aim of this study is to combine the natural microseismicity and groundwater level fluctuations observations to estimate the fault criticality.

To this end, the objectives are to :

- Monitor microseismicity of several strike-slip fault in the Jura Mountains;
- Have continuous **spring discharge** and water table **measurements** of the major karstic springs in the vicinity of the faults;
- Determine **relations** between increasing **spring discharge** rates and **low magnitude earthquakes**;
- Develop a **straightforward methodology** to assess fault criticality.
- Generate stress models of the shallow earth's crust based on field data

Theoretical Background

A) In a mature **karst aquifer**, channeling effects allows large and rapid water table fluctuation resulting in a **rapid and important increase in fluid pressure**. This has a direct **effect on discharge rates** at karstic springs.

B) An **increasing fluid pressure** in the deep aquifers and in the fault zone changes the stress-regime by **reducing the effective normal stress**, leading to the shifting of the Mohr circle towards the Coulomb failure envelope.

C) **Fault slip** affects the fault's transmissivity leading to **fluid flow changes**

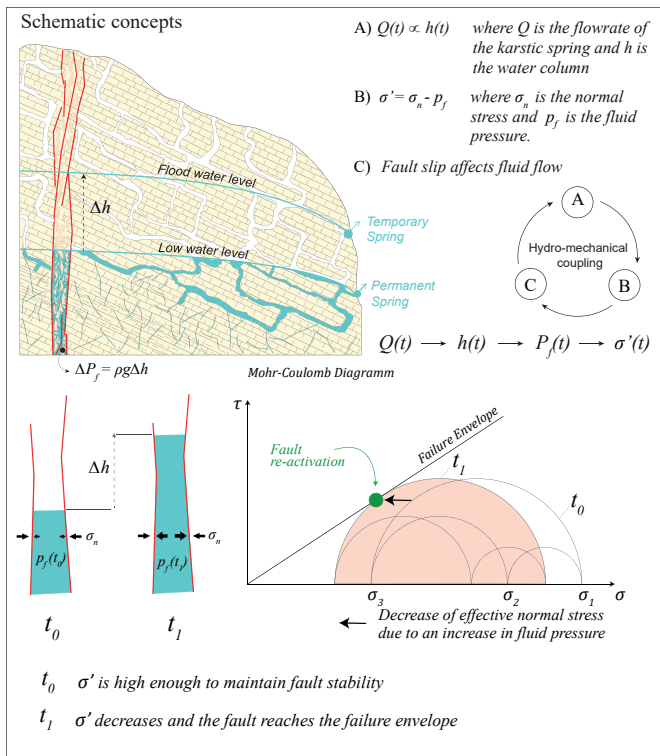


Figure 1 Schematic concept of how karst channeling can influence fluid pressure and consequently the effective normal stress, which can lead to failure and affect the fault's transmissivity and change fluid flow.

Research site, Methods & Data acquisition

The research is carried out on two major strike-slip faults on the northern shore of lake Neuchâtel - La Lance Fault and La Ferrière Fault. Data acquisition mainly consists in (1) hydrogeologic and (2) seismic monitoring.

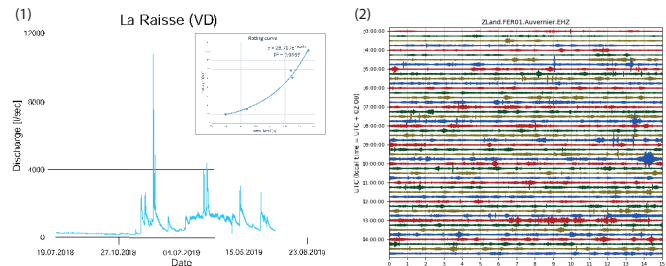


Figure 2 (1) 1-year high resolution discharge ratios of the La Raisse Spring near Vaumarcus and the rating curve. (2) 12-hours (16.07.2019) recording plot of a 3-Channel geophone installed in Auvierier.

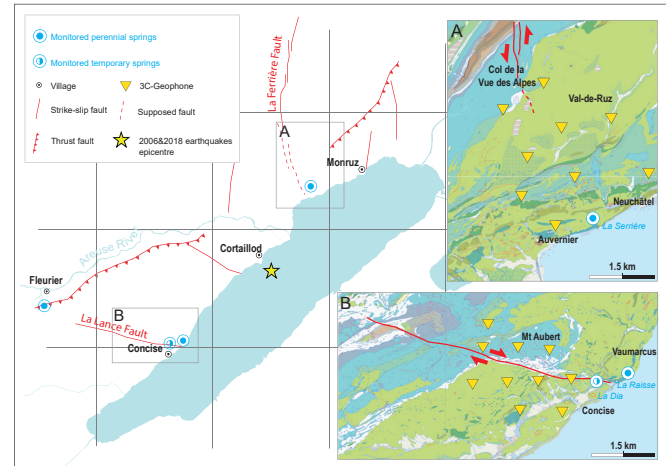


Figure 3 Situation map of the research area. Showing major strike-slip and thrust faults in red, monitored karstic springs and future position of the 3C-geophones. Also shown, epicentre of 2006 and 2018 events (see next section). Data from the geologic and hydrogeologic map [2].

Project Status & Future work

- The hydrogeologic and part of the seismic monitoring stations are in place and **data acquisition on-going**
- **First observations** on historical data [3] revealed two earthquakes with $M_L = 3.2$ (2006) and $M_L = 1.1$ (2018) occurring during flowrates of 1-year return period for the Areuse River (60-70 m³/s). Both events have same epicentre and source (according to waveform similarity theory [4]). Future data will allow more correlation.
- Correlation of seismic patterns with specific flowrates will be used to **develop a quantitative knowledge of what pressure change is affecting fault stability**. This will allow to better constrain the stresses in the Neuchâtel Jura.

Acknowledgments

The project is financially supported by swisstopo and the Swiss Federal Office of Energy.

References

- [1] Miller S.A. (2008) Note on rain-triggered earthquakes and their dependence on karst geology, Geophysical Journal International, Volume 173, Issue 1, pages 334-338
- [2] <https://map.geo.admin.ch> Geocover and hydrogeologic map.
- [3] Swiss Seismological Service (SED), <http://www.seismo.ethz.ch>
- [4] Geller R. & Mueller C. (1980) Four similar earthquakes in Central California, Geophysical Research Letters, 7, 821-824

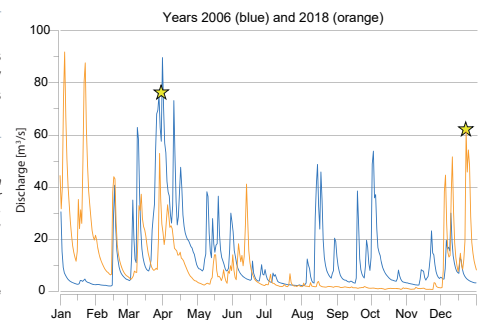


Figure 4 Areuse discharge ratios for 2006 and 2018. Yellow star = earthquake

Anomalous Vp/Vs in pressurized reservoirs: Does it exist and what does it entail?

Lucas Pimienta¹, Beatriz Quinta², Eva Caspari², & Marie Violay¹

¹Laboratory of Experimental Rock Mechanics, EPFL, Lausanne, Switzerland

²University of Lausanne, Lausanne, Switzerland

Motivation

Either for prospection or monitoring purposes, one needs to understand the reservoir rocks at depths and its evolution, i.e. the realm of geophysical methods. Field seismics is one main tool that allows enhanced understanding of reservoir rocks at depths. One infers rocks, fluids and their pressure states from the measured seismic attributes: P- and S-wave velocities and attenuations. However, the method relies on a full understanding of the intrinsic elastic properties of fluid saturated rocks and their seismic signature at depth.

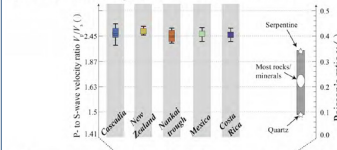
P- to S-wave velocity ratio is an attractive property that directly links to rocks Poisson's ratio, an intrinsic property. However, this property is heavily affected by the frequency of measurements (Pimienta et al., 2016; 2017). Thus, the exact same fluid-saturated rock will exhibit very different Vp/Vs if measured with different methods. In the low frequency range relevant to the field scale, Vp/Vs was shown to reach anomalous values of above 2.5 (Pimienta et al., 2018). Here, we aim at investigating the Vp/Vs expected for different reservoir rocks, from the non-porous granites to the high-porosity sandstones.

Project:

- PROGRESS:** PROspection and PROduction of Geothermal REServoirs
Understand the links between physical properties in geothermal reservoir rocks, & get insights for properties at the field scale.

Principle & Method

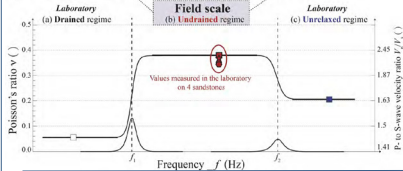
a) Low frequency Vp/Vs in LVZ subduction zones



Anomalous high Vp/Vs have been observed in nature (Fig. a), in subduction zones (e.g. Audet et al., 2009).

Field's measurements are at a frequency of about 1-100 Hz, mostly relevant to the undrained elastic regime (Fig. b).

b) Frequency dependent Poisson's ratio in the laboratory

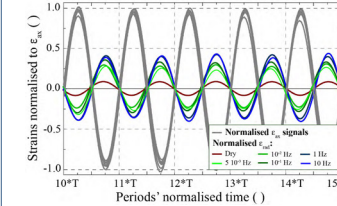


In isotropic rocks, Vp/Vs links to Poisson's ratio when strain amplitudes are small.

Results : Non-porous rocks

Within the framework of the stress-strain methods, the Poisson's ratio is measured, as a function of frequency, as the ratio of radial-to-axial strains.

a) Normalised raw strain oscillations

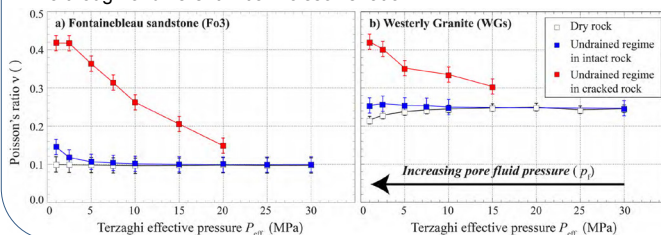


Here, for normalized axial strain, radial strain increases as frequency increases.

Measured Poisson's ratio at a given pressure is inferred from each oscillations, at frequencies relevant to the undrained regime.

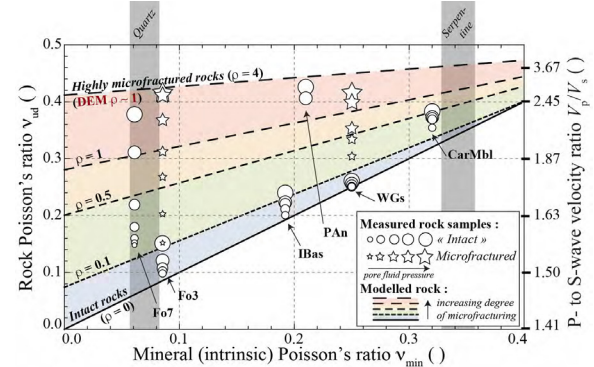
From measuring rocks, either dry or undrained, one gets:

- Under dry conditions: Slight dependence on Terzaghi effective pressure.
- Under water-saturated undrained conditions:
 - "Intact" rock: Slight effect of pressures
 - "Cracked" rock: Large decrease with increasing effective pressure (by decreasing pore fluid pressure), starting from values above 0.4 although of different initial Poisson's ratio!



For non-porous rocks, consistent with inclusions models for effective medium theory:

Independent of the mineral matrix, Poisson's ratio increases as the concentration of cracks opened by high pore fluid pressure increases.

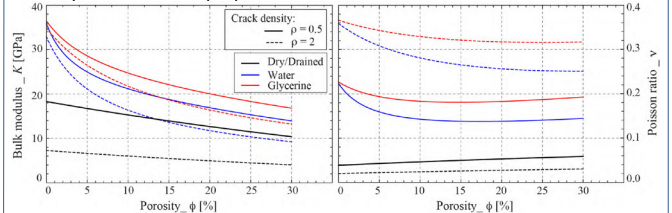


Discussion: High-porosity rocks

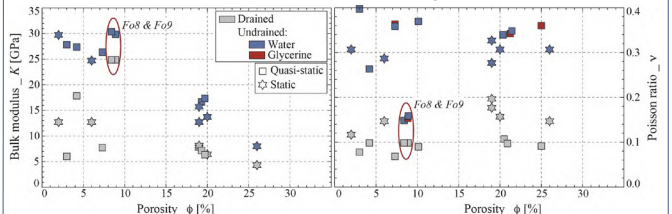
For current strategies to both enhance geothermal systems and heat fluids, tracking seismic Vp/Vs might give insights on the fracture networks and whether they are open or closed.

However, because they would bear much larger permeability, attractive reservoirs rocks for geothermal energy applications need to be porous. It is then of interest to question which Vp/Vs one would get in heavily microcracked rocks. Indeed, owing to their genesis, many sandstones naturally bear open microcracks or grain contacts.

From existing inclusion models of effective medium theories, the effect of two families of pores on the bulk modulus and Poisson's ratio can be predicted for fluids of different compressibility (air, water or glycerine). As the amount of spherical pores (i.e. "porosity") increases, large decreases are expected for both properties.



However, compiling data found in the literature shows that although large decrease in bulk moduli are indeed observed, no clear variations in Poisson's ratio can be inferred. Moreover, no effect of fluid compressibility is observed either, implying deviations from standard theories. A possible explanation is the anisotropic stress solicitation applied on the poroelastic material, similar to that induced by P-waves.



References

- Audet, P., Bostock, M. G., Christensen, N. I., & Peacock, S. M. (2009): Seismic evidence for overpressured subducted oceanic crust and megathrust fault sealing, *Nature*, **457**(7225), 76–78.
- Pimienta, L., Fortin, J., & Guéguen, Y. (2016): Effect of fluids and frequencies on the Poisson ratio of sandstones, *Geophysics*, **81**(2), D35-D47.
- Pimienta, L., Borgomano, J.V.M., Fortin, J., & Guéguen, Y. (2017): Elastic Dispersions and Attenuations in fully saturated sandstones: Role of mineral content, porosity and pressures, *Journal of Geophysical Research*, **122**(12), 2169-9356.
- Pimienta, L., Schubnel, A., Violay, M., Fortin, J., Guéguen, Y. & Lyon Caen, H., (2018): Anomalous Vp/Vs ratios at seismic frequencies might evidence highly damaged rocks in subduction zones, *Geophysical Research Letters*, **45**.

Effects of fracture connectivity on Rayleigh wave dispersion

Gabriel Quiroga, J. Germán Rubino, Santiago Solazzi, Nicolás Barbosa, and Klaus Holliger

Introduction

Passive seismic sensing is widely used in the monitoring of hydrothermal reservoirs to assess the risks that may derive from their exploitation and stimulation (Taira et al., 2018; Obermann et al., 2015). One key factor in geothermal reservoirs is fracture connectivity. Changes in this parameter have effects on seismic attenuation, anisotropy, and velocity (Rubino et al. 2016). In this work, we studied the effects of fracture connectivity on Rayleigh wave dispersion accounting for frequency-dependent poroelastic effects. This may allow the use of seismic data for a better evaluation of geothermal reservoirs.

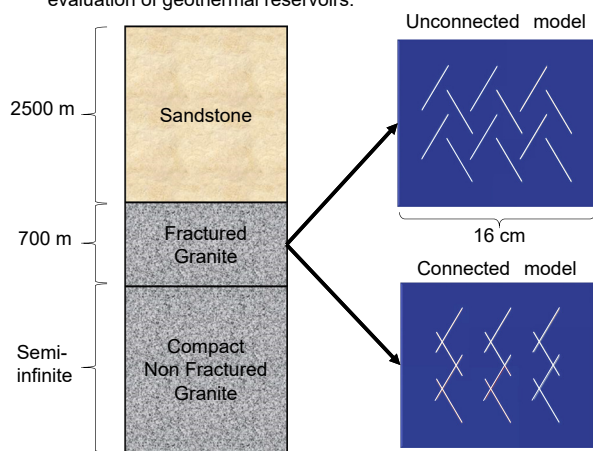


Figure 1. Schematic illustration of the considered three-layer model. The panels on the right show representative samples associated with the fractured reservoir models analyzed in this work.

Methodology and results

We used an upscaling approach based on Biot's poroelasticity theory (Rubino et al. 2016, Hunziker et al. 2018) to determine the effective properties of a water-saturated granite with an unconnected and a connected fracture network (Figure 1). This procedure is used to obtain body wave velocities taking into account fluid pressure diffusion effects (Figure 2).

Using the body wave velocities obtained with the upscaling procedure we implement two reservoir models (Table 1). To obtain the Rayleigh wave dispersion for these models (Figure 3) we used the Geopsy software, which is based on a propagation matrix method (Wathelet 2005, 2011).

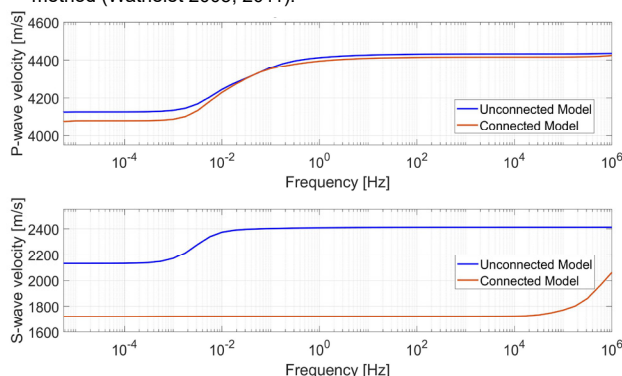


Figure 2. P- and S-wave velocity as a function of frequency for the connected and unconnected granite samples. The frequency range of interest for the Rayleigh wave analysis is highlighted in yellow. It can be appreciated that the relative velocity variation in this region is smaller than 5%, thus allowing the use of constant P- and S- wave velocity values.

Unconnected model

| Layer thickness [m] | Vp [m/s] | Vs [m/s] | Density [kg/m ³] |
|---------------------|----------|----------|------------------------------|
| 2500 | 3500 | 2000 | 2500 |
| 700 | 4430 | 2410 | 2750 |
| Infinite | 5040 | 2620 | 2770 |

Connected model

| Layer thickness [m] | Vp [m/s] | Vs [m/s] | Density [kg/m ³] |
|---------------------|----------|----------|------------------------------|
| 2500 | 3500 | 2000 | 2500 |
| 700 | 4310 | 1720 | 2750 |
| Infinite | 5040 | 2620 | 2770 |

Table 1. Parameters used for the Rayleigh wave dispersion analysis. Values for the second layer result from the upscaling procedure illustrated in Figure 2.

Conclusions

The Rayleigh wave dispersion exhibits a significant sensitivity to fracture connectivity and thus could be used to monitor fracture connectivity as well as related properties of reservoirs.

For different rock types and fracture models, poroelastic attenuation peaks might fall in the frequency range of interest for Rayleigh wave analysis. In these cases, it would be necessary to consider a non-elastic model for the analysis.

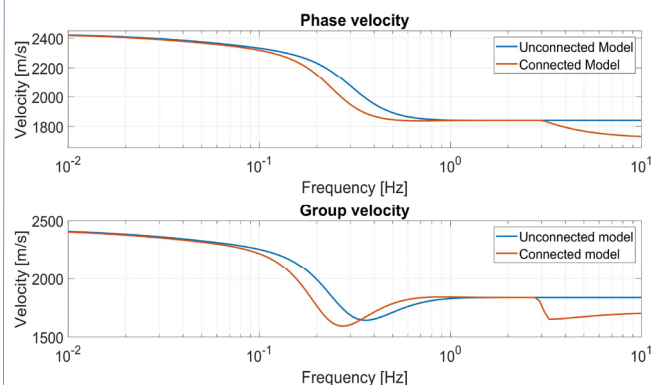


Figure 3. Rayleigh wave dispersion for the connected and unconnected models as functions of frequency. The curves were generated using the GPDC program of the Geopsy applications.

References

- Hunziker, J., Favino, M., Caspari, E., Quintal, B., Rubino, J. G., Krause, R., & Holliger, K. (2018). Seismic attenuation and stiffness modulus dispersion in porous rocks containing stochastic fracture networks. *Journal of Geophysical Research: Solid Earth*, 123(1), 125-143.
- Obermann, A., Kraft, T., Larose, E., & Wiemer, S. (2015). Potential of ambient seismic noise techniques to monitor the St. Gallen geothermal site (Switzerland). *Journal of Geophysical Research: Solid Earth*, 4301-4316.
- Rubino, J. G., Caspari, E., Müller, T. M., Milani, M., Barbosa, N. D., & Holliger, K. (2016). Numerical upscaling in 2-D heterogeneous poroelastic rocks: Anisotropic attenuation and dispersion of seismic waves. *Journal of Geophysical Research: Solid Earth*, 121(9), 6698-6721.
- Taira, T., Nayak, A., Brenguier, F., & Manga, M. (2018). Monitoring reservoir response to earthquakes and fluid extraction, Salton Sea geothermal field, California. *Science Advances*, 4(1), e1701536.
- Wathelet, M. (2005). Array recordings of ambient vibrations: surface-wave inversion. Phd. Thesis, Faculté des Sciences Appliquées, Université de Liège
- Wathelet, M. (2011). Geopsy project. Software, LGIT, Grenoble, Fr.

Seismic signatures of porous rocks containing partially saturated fracture networks

Santiago G. Solazzi, Jürg Hunziker, Eva Caspari, Marco Favino, and Klaus Holliger

Motivation

A great variety of problems and applications throughout the Earth, environmental, and engineering sciences are concerned with detecting and monitoring the displacement of immiscible fluid phases in fractured geological formations. Given that seismic waves tend to be significantly affected by the presence of hydraulic and mechanical heterogeneities, the seismic method may permit to better characterize partially saturated and fractured environments. In this work, we explore the behaviour of seismic attenuation and phase velocity dispersion due to mesoscopic wave-induced pore fluid pressure diffusion in a brine-saturated porous rock containing a fracture network. We analyse these seismic signatures before and after a CO₂ invasion process. Our results suggest that information about the presence and, more importantly, about the spatial distribution of the CO₂ plume can be retrieved based on the analysis of time-lapse seismic data.

Methodology

- We consider a porous medium that contains an anisotropic stochastic fracture network with a backbone, that is, a connected path for fluid flow (Hunziker et al., 2017). Fracture dip is limited to angles between 30° and 150°, where 0° denotes a vertical fracture and 90° a horizontal one.
- An invasion percolation procedure is employed to simulate the CO₂ displacement through the initially brine-saturated fractured medium (Masson & Pride, 2004). We perform a Monte Carlo analysis of the resulting fluid distribution considering pseudo-random invasion potentials within the fractures.
- We use a numerical upscaling procedure based on poroelasticity theory to obtain the seismic attenuation and phase velocity dispersion of a sub-sample of the medium for different frequencies (Rubino et al., 2016).

Results

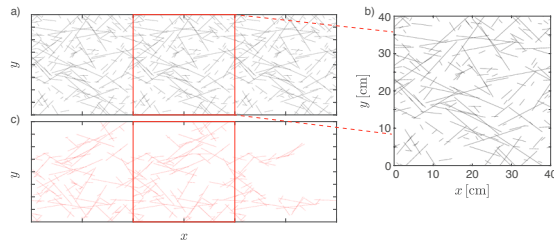


Figure 1: (a) Fracture network considered in the flow simulations and (b) sub-sample considered when exploring the seismic signatures. (c) CO₂-invaded fractures (red) resulting from a single invasion percolation realization.

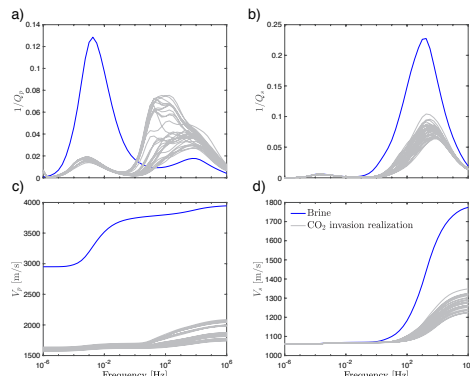


Figure 2: Inverse quality factor and phase velocity as functions of frequency for (a) and (c) P- and (b) and (d) S-waves travelling in the y-direction. We illustrate the fully brine-saturated scenario (blue line), which represents the seismic response prior to the invasion, and 32 curves associated with different invasion percolation realizations (grey lines).

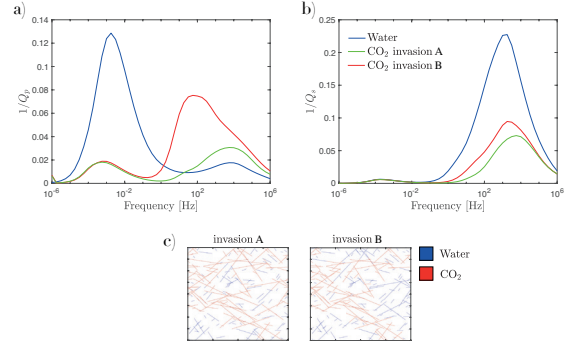


Figure 3: Inverse quality factor as a function of frequency for (a) P- and (b) S-waves for the brine-saturated scenario (blue line) and after two invasion percolation realizations with contrasting characteristics, invasions A (green line) and B (red line). Panel (c) illustrates the fluid distributions associated with the considered models.

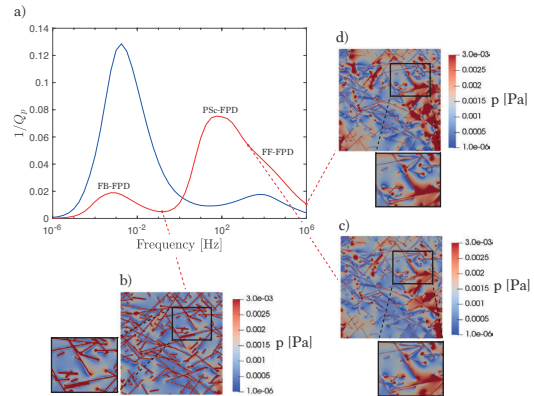


Figure 4: (a) Inverse quality factor as a function of frequency for the fully brine-saturated scenario (blue line) as compared to the partially saturated scenario generated by invasion B (red line). Labels over the attenuation peaks refer to the prevailing fluid pressure diffusion process (FPD), namely, fracture-to-background (FB), partially saturated clustering (PSc), and fracture-to-fracture (FF) flow. Panels (b), (c), and (d) illustrate the pressure fields associated with 0.1 Hz, 1E3 Hz and 1E6 Hz.

Conclusions

In this work, we have analysed the effects partial saturation on a porous rock containing a fracture network. Our results show that the presence of CO₂ in fractures can significantly reduce the phase velocity, particularly for P-waves. We also note that, for P-waves, dissipation levels due to fracture-to-background are reduced and the corresponding effects due to fracture-to-fracture flow are enhanced when compared to the brine saturated scenario. Conversely, we observe a reduction in the attenuation levels due to fracture-to-fracture flow after CO₂ invasion for S-waves. Interestingly, information regarding the fluid distribution within the fracture network is also present in the seismic signatures. Particularly, when CO₂ is not evenly distributed throughout the probed rock sample, P-waves are affected by a new fluid pressure diffusion process taking place between partially saturated and brine saturated zones.

References

- Hunziker, J., Favino, M., Caspari, E., Quintal, B., Rubino, J. G., Krause, R., & Holliger, K. (2018). Seismic attenuation and stiffness modulus dispersion in porous rocks containing stochastic fracture networks. *J. Geophys. Res.*, 123(1), 125-143.
- Masson, Y & Pride, S. R. (2014). A fast algorithm for invasion percolation, *Transp. Porous Med.*, 102(2), 301-312.
- Rubino, J. G., Caspari, E., Müller, T. M., Milani, M., Barbosa, N. D., & Holliger, K. (2016). Numerical upscaling in 2D heterogeneous poroelastic rocks: Anisotropic attenuation and dispersion of seismic waves, *J. Geophys. Res.*, 121, 6698-6721.

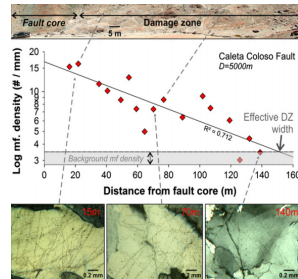
Poroelastic effects of the damaged zone on fracture reflectivity

Edith Sotelo, Santiago G. Solazzi, J. Germán Rubino, Nicolás D. Barbosa, Klaus Holliger

Motivation

Studies show evidence of a zone of microfractures surrounding fractures and faults.

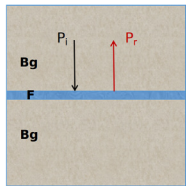
Figure 1. Microfracture density versus distance from fault core and thin sections below. Modified from Mitchell and Faulkner (2012).



Hydraulic changes of the damaged zone can promote fluid pressure diffusion from the fracture as seismic waves travel through the system. This process, together with the damaged zone mechanical weakening are expected to affect the reflectivity of the system.

Methodology

a) Reference model



b) Model with damaged zone

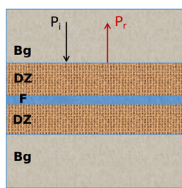


Figure 2. Reference model and model with damaged zone.

- P_i is the normally incident fast P-wave. P_r is the reflected P-wave.

- Bg is the background rock, DZ is the damaged zone and F is the fracture.

We compute the reflection coefficients at the F-Bg interface (Figure 2a) and the DZ-Bg interface (Figure 2b), respectively.

To find amplitudes, we formulate a system of equations by setting continuity of traction and pressure as well as continuity of solid and relative fluid displacements at each interface.

Following Barbosa et al. (2016), we use Biot's theory (Biot, 1962) to formulate pressures, tractions, and displacements since it accounts for fluid pressure diffusion effects.

Results

| Property | Background | Fracture |
|-----------------------------------|------------|----------|
| Permeability (D) | 10^{-6} | 100 |
| Grain bulk modulus (GPa) | 36 | 36 |
| Grain density (g/cm^3) | 2.7 | 2.7 |
| Porosity | 0.15 | 0.8 |
| Frame bulk modulus (GPa) | 9 | 0.056 |
| Frame shear modulus (GPa) | 7 | 0.033 |
| Tortuosity | 3 | 1 |
| Thickness (m) | - | 0.001 |
| Fluid density (g/cm^3) | 1 | |
| Fluid bulk modulus (GPa) | 2.25 | |
| Fluid viscosity (P) | 0.01 | |

Table 1. Reference model properties according to Barbosa et al. (2016)

Unless stated otherwise, the properties of the damaged zone are the same as those of the background except for permeability.

Sensitivity to permeability and thickness of the damaged zone

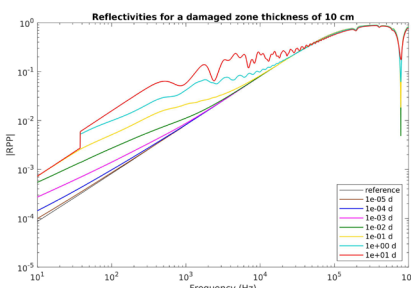


Figure 3. P-wave reflectivity for a model with a damaged zone of 10 cm thickness and with different values of permeability.

Reverberations at high frequencies can be associated with scattering within the damaged zone and the fracture.

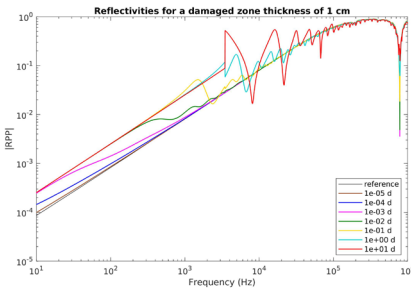


Figure 4. P-wave reflectivity for a model with a damaged zone of 1 cm thickness and with different values of permeability.

Effect of decreasing the damaged zone mechanical properties

We decrease the frame bulk and shear moduli of the damaged zone by 20%, 50%, and 80% with respect to its reference values (background, Table 1). The thickness of the damaged zone is 10 cm.

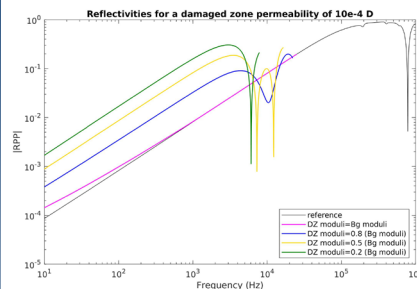


Figure 5. P-wave reflectivity for models with weaker damaged zones, and with a permeability of 10^{-4} D.

The truncation of curves is associated with numerical issues in the matrix inversion.

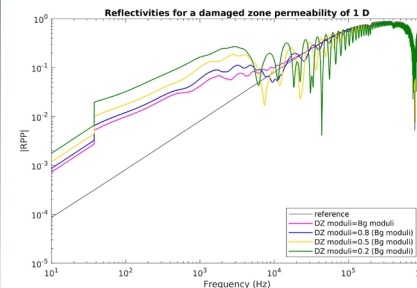


Figure 6. P-wave reflectivity for models with weaker damaged zones, and with a permeability of 1 D.

Jumps at lower frequencies may suggest a background-damaged zone fluid interaction, but further investigation is needed to explain this behavior.

Discussion and Conclusions

As shown in Figures 3 and 4, accounting only for the permeability enhancement associated with the damaged zone increases the reflectivity. This effect is explained by the increase of fracture compliance when fluid pressure diffusion occurs from the fracture to the damaged zone.

As shown in Figures 5 and 6, mechanical weakening of the damaged zone increases the reflectivity, thus showing the effect of enhancing the mechanical contrast with the background.

Further studies are needed to fully assess the presence of reverberations at higher frequencies, jumps at lower frequencies, and of other local features in the reflectivity curves.

Reference

Barbosa, Nicolás D., et al. (2016) "Fluid pressure diffusion effects on the seismic reflectivity of a single fracture." The Journal of the Acoustical Society of America 140(4), 2554-2570.

Biot, M. A. (1962). "Mechanics of deformation and acoustic propagation in porous media." Journal Applied Physics 33, 1482–1498.

Mitchell, T. M., and D. R. Faulkner (2012). "Towards quantifying the matrix permeability of fault damage zones in low porosity rocks." Earth and Planetary Science Letters 339, 24-31.

Where are the favorable locations for deep geothermal in Switzerland ?

Benoît Valley & Stephen A. Miller

Centre for Hydrogeology and Geothermics (CHYN), University of Neuchâtel, Switzerland
 benoit.valley@unine.ch

Motivation

We know conceptually what features constitute favorable targets for geothermal projects (Fig. 1), however optimally targeting projects remains challenging. Numerous data sets have been compiled over the last few years to assist geothermal exploration.

- How can we combine these data to identify favorable locations for geothermal projects ?
- What limitations exists in our data and method to successfully target deep geothermal projects ?

The objective of this contribution is to answer these questions by an attempt to compute a geothermal favorability index for the Swiss plateau based on the currently available data.

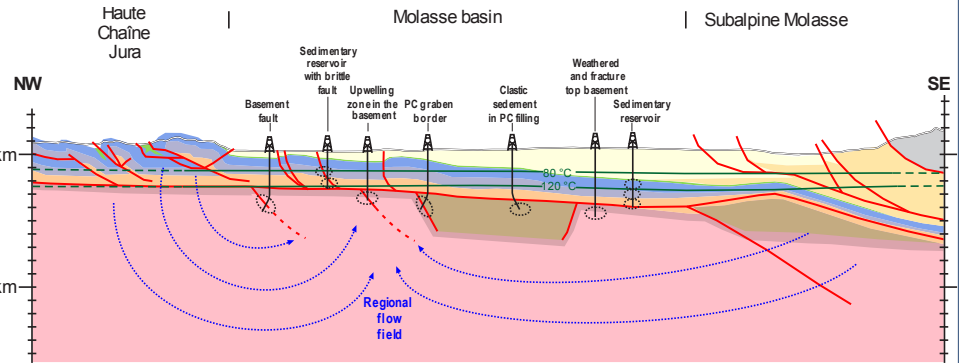


Figure 1: Cross-section through the Swiss plateau after Burkhard and Sommaruga (1998) with a representation of the conceptual targets for deep geothermal.

Data set

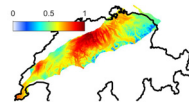
In this work we compiled and combined the following data sets and information:

- Hydrostratigraphy (Chevalier et al. 2010)
- Mechanical stratigraphy (Hergert et al., 2015)
- Geomol horizon model (swisstopo)
- Geomol fault model (swisstopo)
- Geomol temperature model (swisstopo)
- Heat flow map (swisstopo)
- Spring and thermal spring locations (Hydr. Atlas of CH, Sonney and Vuataz, 2008)
- Evaluation of regional flow pattern
- Stress field estimation with a Swiss-scale finite element stress simulation
- Earthquake catalog of Switzerland (download from SED website)

We defined 11 favorability criteria computed from one or a combination of the datasets listed above. For each criteria a favorability index ranging from 0 (=unfavorable) to 1 (=favorable) was computed. We performed our analyses on a 1km x 1km grid covering the extend of the geomol model. In addition, we focus on two specific temperature levels: 80°C and 120°C, being the typical minimum temperature level for direct use and electricity production, respectively. We show here the results of the computation for the 80°C temperature target.

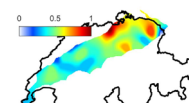
Criteria 1: depth to target temperature

We give higher favorability when the target temperature of 80°C is reached at shallower depth.



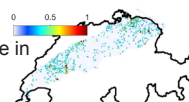
Criteria 2: heat flow

High heatflow is indicative of enhanced heat transport through advection and thus area with higher heat flow are rated with a higher favorability index



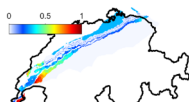
Criteria 3: Seismic event density

Higher seismic density are associated with damage in the crust and fluid flow. We give thus higher favorability for area with higher seismic events density. We recognize that seismic risk must be assessed separately



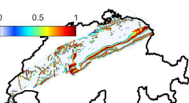
Criteria 4: Lithological control

Impervious lithologies (aquicludes) are unfavorable while aquifer formation favorability are rated according to the aquifer thickness (thick aquifer are most favorable).



Criteria 5: distance to faults

Faults enhance rock mass damage favoring permeability. Location close to faults are rated favorably.

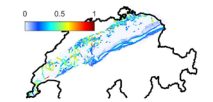


Acknowledgements

We acknowledge the support from R. Reynolds and R. Allenbach from swisstopo in providing the geomol structural and temperature datasets. B. Valley is supported by the Swiss Competence Center for Energy Research (SCCER-SoE).

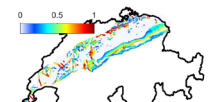
Criteria 6: Slip tendency

Critically stressed faults with high slip tendency are considered favorable to host deep seated fluid flow. We combined here the stress model and the fault data to give higher favorability to location close to faults with high slip tendency.



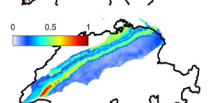
Criteria 7: Dilation tendency

Location close to faults with low normal stress (high dilation tendency) are rated favorably.



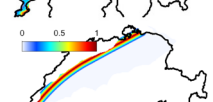
Criteria 8: Von Mises stress

Stiff formation attracting stresses will be more fractured and thus are rated more favorably. We derive this index from the stress model results.



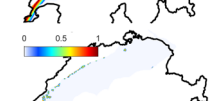
Criteria 9: Regional flow pattern

Regional high recharge area (downward flow) are rated less favorably than regional discharge areas.



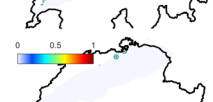
Criteria 10: Regional springs

The proximity of regional spring is indicative of water flow pathways and thus rated as favorable



Criteria 11: Thermal springs

Thermal springs denote up flow area and are indicative of favorable conditions for geothermal projects.



Combined favorability index

The combination of all criteria is shown on Fig. 2. Sharp contrast in favorability can be highlighted on the Swiss plateau and these contrasts can guide exploration. However, this as to be considered as a preliminary approach and also at a scale that is not appropriate for local scale exploration planning. Future approaches will include a more careful analyses of the elements leading to the combined favorability map. Another important element will be to include data from exploration projects in order to based the weighting scheme on a more robust ground. The methodology and results presented here are bound to evolve when more data becomes available.

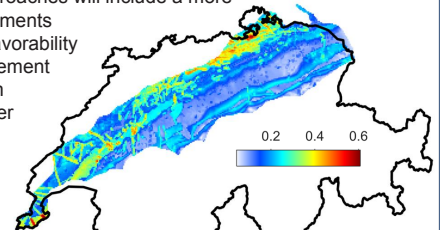


Figure 2: Combined favorability index for 80°C geothermal targets.

References

- Burkhard M, Sommaruga A (1998) Evolution of the western Swiss Molasse basin: structural relations with the Alps and the Jura belt. *Geol Soc Lond Spec Publ* 134:279–298. doi: 10.1144/GSL.SP.1998.134.01.13
- Chevalier G, Diamond LW, Leu W (2010) Potential for deep geological sequestration of CO₂ in Switzerland: a first appraisal. *Swiss J Geosci* 103:427–455. doi: 10.1007/s00015-010-0030-4
- Hergert T, Heidbach O, Rüter K, et al (2015) Stress field sensitivity analysis in a sedimentary sequence of the Alpine foreland, northern Switzerland. *Solid Earth* 6:533–552. doi: 10.5194/se-6-533-2015
- Sonney R, Vuataz F-D (2008) Properties of geothermal fluids in Switzerland: a new interactive database. *Geothermics* 37:496–509

Geochemical evidence for large-scale and long-term topography-driven groundwater flow in orogenic crystalline basements

Christoph Wanner¹, H. Niklaus Waber¹, Kurt Bucher²

¹Rock–Water Interaction, Institute of Geological Sciences, University of Bern

²Mineralogy and Petrology, University of Freiburg, Germany

Motivation

Orogenic belts without active igneous activity are recognized as plays for geothermal energy. In these systems, meteoric water circulation is typically expressed by thermal springs discharging at temperatures up to 70 °C from deep-reaching faults. The hydraulic gradients that drive circulation arise from the conjunction of high orographic precipitation, mountainous topography and permeable faults that link topographic highs with valley floors via the hot bedrock. Since the bedrock geotherm is the only source of heat for the circulating water, its maximum depth of penetration defines the maximum temperature attainable by surface springs and their upflow zones, thereby setting limits on their potential for geothermal energy exploitation. In the framework of the SCCER-SoE Task 1.1 we have conducted large-scale (20 x 10 x 9 km) thermal-hydraulic-chemical (THC) simulations of meteoric water circulation within a selected domain of the Aar Massif hosting the Gotthard railbase tunnel in the Central Alps, Switzerland, to better understand THC processes in orogenic crystalline basements and to assess their role in generating exploitable heat anomalies.

Geological and hydrogeochemical constraints

- Study relates to the Amsteg section of the Gotthard railbase tunnel with steeply dipping granitic rock units and fracture systems
- 122 groundwater samples were collected during tunnel construction (2003–2006) and subsequently analyzed (Bucher et al., 2012)
- Stable water-isotope analyses reveal a meteoric fluid origin
- Water samples collected beneath the only major valley of the section, the Maderaner Valley, are supersaturated with respect to chalcidony
- This is a typical feature of ascending thermal waters and indicates that these samples have infiltrated into the tunnel from below
- A distinct salinity peak (e.g. [Cl]) appears at ca. 10 km along the tunnel, roughly consistent with the identified upflow zone
- Matrix porewater (i.e. remnants of ancient hydrothermal fluids) is the most likely Cl source. [Cl] may thus operate as a residence time tracer
- Low [Cl] beneath major mountain peaks (e.g. Chrüzlistock) suggest short residence times and hence infiltration into the tunnel from above
- The postulated up- and downflow zones are consistent with the occurrence of two distinct water types along the tunnel (see Fig. 1f)
- Water temperatures correlate with overburden and do not show any anomalies

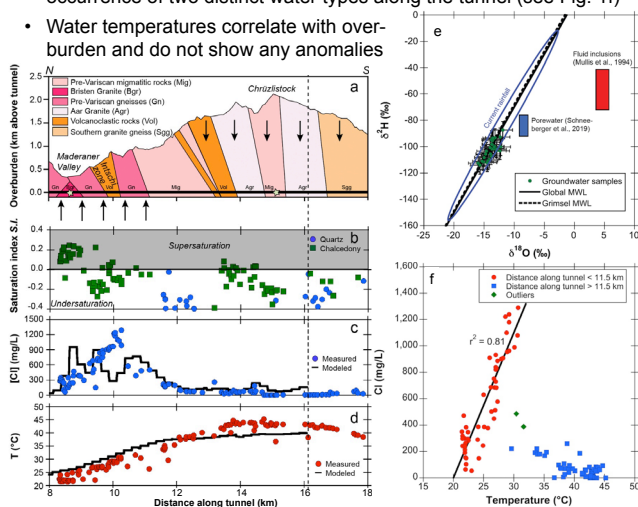


Fig. 1: Profiles along the Amsteg section of the Gotthard railbase tunnel. (a) Geological units and flow zones inferred from geochemical constraints. (b) Saturation indices of quartz (pH>9.5) and chalcidony (pH<9.5) in groundwater samples. (c) Measured and computed [Cl] of groundwater samples. (d) Measured and computed temperatures of groundwater samples. (e) Stable O-H isotope signatures of 30 groundwater samples. (f) [Cl] of all 122 groundwater samples plotted against their discharge temperature.

Model setup

- Horizontal extent constrained by the catchment of the Maderaner Valley
- Upper model boundary specified based on digital elevation model
- Fixed P and T at upper model boundary (1 bar, 4 °C)
- Initial conductive temperature distribution considering a geothermal gradient of 25 °C/km; initial hydrostatic P distribution
- Depth dependent permeability and porosity (Stober & Bucher, 2015)
- Uptake of Cl abstracted by defining a hypothetical $\text{NaCl}_{(s)}$ source with a fixed dissolution rate ($\text{NaCl}_{(s)} = \text{Na}^+ + \text{Cl}^-$)

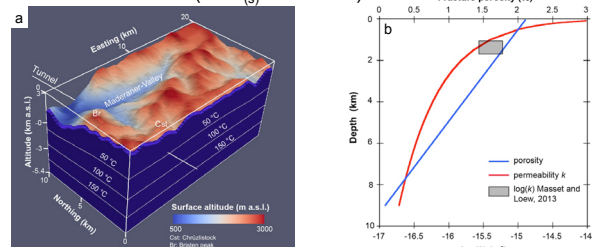


Fig. 2: (a) Model geometry and initially specified conductive temperature distribution. (b) Specified depth-dependent porosity and permeability distribution.

Results and discussion

- Model predicts downflow ($v_z < 0$) of meteoric water at high altitude, and upflow ($v_z > 0$) beneath major valleys (Fig. 4a)
- Meteoric water infiltrating at the surface reaches the lower model boundary and hence attains $T > 150$ °C (Fig. 4b)
- Despite such deep circulation, the model predicts only a minor T anomaly beneath the Maderaner Valley (see 50 °C isotherm)
- The model is able to capture observed [Cl] and temperatures, as well as up- and downflow zones identified from geochemical constraints (Fig. 1)
- The model predicts slow upflow rates below 2 m/year. Such low water fluxes, is the likely reason major thermal anomalies are absent
- Slow water circulation also results in residence times that may exceed 100'000 years (Fig. 3)

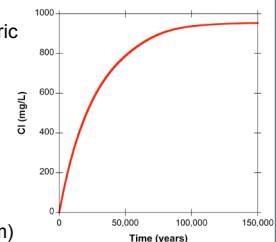


Fig. 3: Simulated Cl breakthrough below the Maderaner Valley.

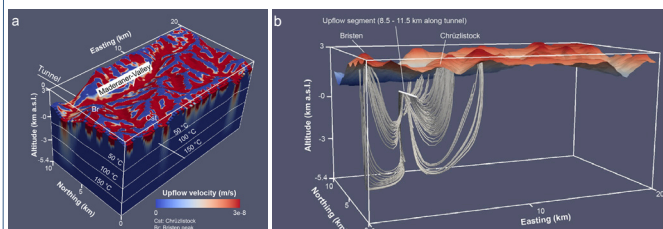


Fig. 4: (a) Upflow velocity distribution (i.e. positive z -component of the computed flow vectors) and steady state isotherms. (b) Streamlines of meteoric water infiltrating at the upper model boundary and discharging into the tunnel along the identified upflow zone (Fig. 1a)

Implications for exploration for orogenic geothermal systems

- Surface topography and meteoric water infiltration form the main controls on fluid flow in orogenic geothermal systems
- Down to 9 km depth, penetration of meteoric water is not limited by the decrease in permeability typical of granitic basement rocks
- Temperature anomalies and hence exploitable geothermal systems preferably form when steeply-dipping, major faults zones with elevated permeability intersect with valley floors

References: Bucher K., Stober I. & Seelig U. (2012). Chem. Geol. 334, 240-253. Massot O. & Loew S. (2013) Eng. Geol. 164, 50-66. Schneebberger R., Kober F., et al. (2019) NTB 19-01. Mullis J., Dubessy J., et al. (1994) Geochim. Cosmochim. Acta 58, 2239-2267. Stober I. & Bucher K. (2015) Geofluids 15, 161-178.